Engineering Structures 279 (2023) 115557

Contents lists available at ScienceDirect

Engineering Structures

journal homepage: www.elsevier.com/locate/engstruct

# Fail-safe optimum cable system under cable breakage in cable-stayed bridges. Application to the Queensferry Crossing Bridge

Noel Soto, Clara Cid *, Aitor Baldomir, Santiago Hernández

*Structural Mechanics Group, School of Civil Engineering, Universidade da Coruña, 15071, Spain*

ARTICLE INFO

*Keywords:*
Cable-stayed bridge
Optimum design
Fail-safe
Cable breakage
Crossing cables

ABSTRACT

This paper presents a methodology to optimize the cable system in cable-stayed bridges, whose main novelty is to take into account the accidental breakage of one cable within the design process. To this end, a multi-model optimization strategy is proposed by establishing design constraints on both the intact and damaged models. The dynamic effect of cable breakage is accounted for in the damaged models by the application of impact loads at the tower and deck anchorages. The objective function is to minimize the steel volume in the cable system by varying the cable anchor positions on the deck, the number of cables, the cross sectional areas and prestressing forces. This approach is applied to the Queensferry Crossing Bridge, the longest three-tower cable-stayed bridge in the world and also the largest with crossing cables in the central spans. The fail-safe optimization of the cable system leads to a different layout than the optimum design without considering cable breakage, with more cables and smaller areas, having a minimum penalty in steel volume.

## 1. Introduction

Cable-stayed bridges have earned a reputation in the civil engineering field for their elegance and ability to span long distances. As a result, the development of optimization techniques applied to these structures has gained prominence in the research community. While there are several papers focused on optimizing the shape or thicknesses of the deck as well as the cable area and prestressing forces [1–8], other researchers have concentrated their efforts on minimizing the weight and arrangement of the cable system. The reason is that a reduction in the steel volume of the cable system can lead to considerable savings, since it represents approximately 10% of the total cost of the bridge, as presented by Sun et al. [9]. In this sense, the determination of the optimum distribution of cable forces has been thoroughly studied [10–21]. Among these works, Baldomir et al. [15,19] obtained the cable areas for long span bridges by minimizing the volume of cables through a gradient-based optimization algorithm considering fixed anchor positions. Later, Cid et al. [22] proposed a methodology to define the optimum cable system in multi-span cable-stayed bridges, allowing crossed cables in the main spans, different number of cables at each side of the towers and different cable areas. A comprehensive summary of the state of the art in cable-stayed bridge optimization was presented by Martins et al. [23] through an extensive literature survey, where 90 articles were chosen for a detailed review.

Recently, several accidents have occurred associated with a cable rupture, such as the Morandi Bridge [24], [25] or the Nanfang'ao Bridge [26]. In both cases, the broken cables were badly damaged due to corrosion in the moment of the collapse, which could indicate that it was the cause of the accident. However, in none of these references it is explicitly stated that corrosion was the cause of the collapse. Nowadays, codes and regulations state that bridges must be safe against accidental failure, since structural damage may lead to a catastrophic event. In this sense, the Post-Tensioning Institute (PTI) [27] specifies that *"cable-stayed bridges shall be capable of withstanding the loss of any one cable without the occurrence of structural instability"*. Most countries have included these recommendations for the design of cable-stayed bridges in their respective regulations. This is the case of the Rego das Lamas Viaduct (Spain), Taney Bridge (Ireland) and Champlain Bridge (Canada). For instance, as stated in the documentary A Giant On The River [28] *"the Champlain Bridge was designed for the loss of up to three stays, simultaneously or consecutively, at any point in the structure [...]. The bridge may not be in sufficiently good condition to permit its use, but the bridge will withstand and can be repaired"*. A design capable of sustaining possible damage is referred to in the literature as a fail-safe design.

Safe-life, fail-safety and damage tolerance are design philosophies that emerged in the aerospace engineering field, aiming for aircraft safety and reliability [29]. In particular, fail-safety aims to design aircraft in which significant structural damage can appear during flight without incurring in a catastrophic event. It is defined in the AC 25.571-1D [30] as "*the attribute of the structure that permits it to retain its required*

* Corresponding author.
*E-mail addresses:* noel.sotom@udc.es (N. Soto), clara.cid.bengoa@udc.es (C. Cid), abaldomir@udc.es (A. Baldomir), hernandez@udc.es (S. Hernández).

https://doi.org/10.1016/j.engstruct.2022.115557
Received 23 July 2022; Received in revised form 11 November 2022; Accepted 27 December 2022
Available online 6 January 2023

*residual strength for a period of unrepaired used after the failure or partial failure of a principal structural element*". The general requirement is that the remaining structure is able to sustain limit loads after failure of any principal structural element, regardless of the source of origin, such as fatigue, cracking, corrosion, accidental damage, manufacturing defects, environmental conditions, and discrete events, such as collisions. In this work, we apply this concept to the civil engineering field, to refer to a bridge design capable of sustaining possible damage. The design that takes this into account is considered to be fail-safe if the remaining structure was conceived to withstand such damage, thus ensuring an adequate redistribution of internal forces. This design philosophy inevitably leads to an increase in structural weight with respect to the conventional design, which will be referred to as penalty weight in this work.

In this regard, two important issues must be taken into account: (1) when designing a fail-safe structure, there is usually a tendency to oversize the final solution, and (2) the aforementioned optimization strategies for cable-stayed bridges do not currently include this design philosophy in their formulation. Thus, finding an improved cable arrangement that can withstand this accidental situation could result in significant cost savings. In this context, the idea of this research was born, which aims to answer the following question: Is there an optimum cable arrangement that could resist the breakage of one cable?

The breakage of a cable produces a dynamic effect that cannot be disregarded in the structural response of the bridge. Therefore, a nonlinear dynamic analysis would be necessary to accurately capture the effect of the cable breakage. However, current guidelines and codes propose a simplification to obtain an approximation of the dynamic response by means of a quasi-static analysis. This requires knowing the force on the cable before breakage and applying that force on the deck and tower multiplied by a dynamic amplification factor (DAF). In this quasi-static analysis, the DAF value is the same for each cable, so the fluctuation of the DAF is not taken into account. In this regard, several authors have conducted comprehensive studies to determine the most adequate value for the DAF. Zoli and Woodward [31] analyzed a tied arch bridge subjected to the loss of a cable and found DAF values between 0.5 and 0.81 for tie girder and arch rib peak stress. Starossek and Wolff [32,33] studied the dynamic response of a two-tower cable-stayed bridge with fan distribution in case of a cable breakage. They found that the DAF strongly depends on the location and type of the cable breakage, as well as the response considered (deflections, bending moments, etc.). They concluded that a conservative value of 2.0 can be used to determine axial forces in cables and bending moments in the deck. However, bending moments in the pylons can produce significantly higher DAFs, so a dynamic analysis should be performed for this case. Cai et al. [34] supported the use of conservative DAF of 2.0 although in this study only deck displacements and cable forces were considered. On the other hand, other authors [35–38] concluded that a DAF higher than 2.0 can be reached in some cases.

To answer the above question, it will be necessary to apply a fail-safe optimization methodology. In that regard, several investigations were carried out in recent years, which can be classified into fail-safe topology and fail-safe size optimization. Fail-safe topology optimization pursues to minimize the compliance of a conceptual design that can sustain damage. It has an enormous potential in early stages of the design process of a structure. Some researchers have analyzed the local failure for truss structures, where the local failure can be modeled straightforwardly by removing one bar from the truss, since a clear definition of a structural member exists [39–41]. Another research line is focused on the fail-safe topology optimization of continuum structures. In this case, the first limitation is the absence of discrete structural elements to be eliminated, as members emerge after performing the optimization process. Thus, damage scenarios are defined in the design domain by eliminating areas or patches of a given size [42–50]. In general, this approach leads to conceptual designs that must be defined in detail in later design phases. It is at this point that size optimization methods gain prominence since they allow minimizing the weight of the structure by determining the mechanical properties of its components. In this case, the topology is not modified, i.e. the connectivity of the elements remains unchanged. What is done is to reinforce the original structure without incorporating additional structural elements. First works in fail-safe size optimization of structures were applied to bar structures [51–54]. Fail-safe size optimization was firstly applied to shell structures by Baldomir et al. [55]. Other relevant works can be found in Refs. [56–62].

This paper presents for the first time a strategy to minimize the weight of cables in cable-stayed bridges considering the dynamic effect of the breakage of any of its cables. As a result the bridge must withstand the loss of any cable without compromising its structural integrity.

The remainder of the paper is organized as follows: Section 2.1 summarizes the general formulation of the fail-safe optimization, and Section 2.2 introduces the simplified approach to represent the cable loss. Then, Section 3.1 presents the FEM used in this research and Section 3.2 formulates the fail-safe optimization of the cable system under cable breakage, providing a detailed description of the method. Section 4 applies the proposed methodology to the Queensferry Crossing bridge, analyzes the optimum cable arrangement and compares it with the optimum solution without considering a sudden cable loss. Finally, Section 5 offers concluding remarks.

## 2. Background

### 2.1. General approach for fail-safe optimization

A general methodology for fail-safe optimization was presented by Baldomir et al. [55]. In that work, a generic FEM and $D$ damaged configurations of the structure were defined, as shown in Fig. 1. An identifier code $M_i$ is assigned to each model, where $i = 0$ corresponds to the intact model and $i = 1, 2, \dots, D$ are the damaged configurations. The vector of design variables is denoted by $\mathbf{x}$, taking the same value in each configuration. In other words, the intact and damaged configurations $M_i$ $(i = 1, \dots, D)$ have the same assignment of design variables. Therefore, when a design variable of the intact model is modified by the optimization algorithm, the same modification is done in the damaged configurations. The main idea is to include into the optimization problem a set of design constraints from both the intact and damaged models. The solution to this problem provides an optimum design that satisfies the constraints in the intact and the entire set of damaged models simultaneously with a minimum penalty weight.

The general formulation of the fail-safe optimization problem is expressed in Eq. (1), where $F$ is the function to be minimized, $\mathbf{x}$ is the vector of design variables, $g_j^{M_i} \leq 0$ refers to the $j$th constraint in the model $M_i$ and $m^{M_i}$ corresponds to the number of constraints applied to $M_i$.

$$\min \; F(\mathbf{x}) \tag{1a}$$

$$\text{s. t.} \quad g_j^{M_i}(\mathbf{x}) \leqslant 0 \quad j = 1, \dots, m^{M_i} \qquad i = 0, \dots, D \tag{1b}$$

### 2.2. Cable breakage

The structural response of a cable-stayed bridge due to the sudden loss of a cable can be calculated either by a non-linear dynamic analysis or by a quasi-static approach. The latter takes into account the dynamic effects by a Dynamic Amplification Factor (DAF), which is defined as the dimensionless ratio between the dynamic response and the static response [63]. Therefore, the cable breakage can be represented in a simplified manner by the static force of the broken cable ($F$) applied to the deck and tower multiplied by the DAF, as shown in Fig. 2.

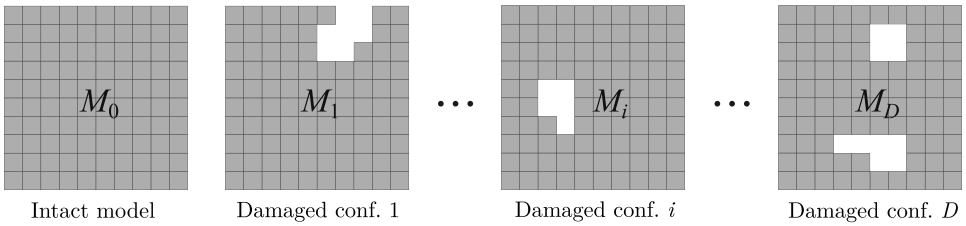


**Fig. 1.** General definition of the intact model and damaged configurations [55].

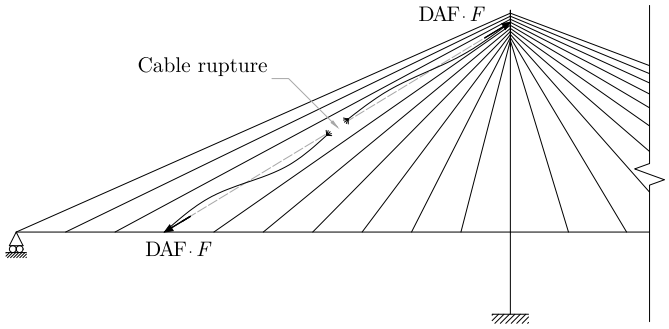


**Fig. 2.** Impact loads due to the loss of a cable.

Due to its simplicity, the existing codes and guidelines have adopted this quasi-static approach in the design of bridges. Among them, the Post-Tensioning Institute (PTI) [27] establishes the load combination to be used in case of accidental cable rupture as well as a DAF equal to 2.0 to represent the cable loss. This value is assumed to be constant, which according to the state-of-the-art is conservative in most cases.

$$1.1 \cdot DC + 1.35 \cdot DW + 0.75 \cdot LL + 1.1 \cdot PS + 1.1 \cdot \underbrace{DAF \cdot F}_{CLDF} \tag{2}$$

where $DC$ represents the dead load of structural components and non-structural attachments, $DW$ is the dead load of wearing surfaces and utilities, $LL$ the vehicular live load, $PS$ the prestressing forces of cables and $CLDF$ the equivalent static force due to a cable loss. This load combination has been used in this work to simulate the cable loss.

## 3. Methodology

### 3.1. Bridge and cable system description

A generic three tower cable-stayed bridge with crossing cables in main spans has been adopted as base model for the formulation of the fail-safe optimization problem. The bridge geometry and the nomenclature used are shown in Figs. 3 and 4. This model was developed in a previous work [22] whose aim was to find the optimum cable system that minimizes the steel volume, considering as design variables the cable anchor positions on the deck, cross-sectional areas and prestressing forces.

As can be seen in Fig. 4, the half of the bridge was divided into four regions: side span, main span tower 1, main span crossing zone, and main span tower 2, where the number of cables in each region can take any value within the interval between square brackets. The number of cables in the half-length of the bridge is represented by $N_C$, which corresponds to the sum of cables in the side span ($N_S$) and cables in the main span ($N_M = N_{M1} + N_{MC1} + N_{MC2} + N_{M2}$). Therefore, the total number of cables in the bridge is $N_T = 2 \cdot N_C$. Cables in the crossing zone are grouped by pairs, sharing the same anchor position on the deck.

A generic 2D finite element model was defined by using the commercial software Abaqus [64] through a Python script. The structural analysis type adopted for the Abaqus FE model was nonlinear, with large displacements (known as P-$\Delta$ effect) and considering cable sag effect.

The connections between cables-deck and cables-tower were designed as tie constraints. In this manner, the connections are independent of the mesh, making it possible that each cable anchor position on the deck can be considered as a design variable without having to update node connectivities.

### 3.2. Fail-safe optimization applied to cable-stayed bridges

This section proposes a new methodology to obtain the optimum cable system in cable-stayed bridges under cable breakage. This means that any cable can suddenly break and none of the design constraints will be violated. For this purpose, the fail-safe methodology described in Section 2.1 is now applied to the work presented by Cid et al. [22], taking into account the dynamic effect of cable breakage described in Section 2.2. A total number of $D$ damaged configurations has been defined as a result of the breakage of a single cable, as shown in Fig. 5. Thus, the number of damaged configurations would be $D = N_T$.

The cable rupture has been modeled in the FEM by reducing its stiffness to a low value ($E = 1$ MPa) and setting a zero density value ($\rho = 0$ t/m$^3$). In this way, the cable anchor nodes are maintained in the model and the impact forces due to the sudden rupture of the cable can be assigned more easily than removing the cable element. As commented in Section 2.2, the structural response in the damaged models must include the dynamic effect of cable breakage, which in this case will be considered by a DAF of 2.0. To do so, the axial force for each cable ($k$) and load case ($l$) without partial safety coefficients have to be previously computed in the intact model, $F_{cable,k}^{M_{0,l}}$. These values will be used to obtain the $CLDF$ to be applied in damaged configurations.

The optimization problem aim to find a configuration that minimizes the steel volume of the cable system subject to structural design constraints. The general formulation of the optimization problem is expressed in Eq. (3), being $V$ the volume of steel in the cable system.

$$\min\ V = 2 \cdot \sum_{k=1}^{N_C} \left( x_k^A \cdot L_k\left(x_k^P\right)\right) \tag{3a}$$

$$\text{s. t.}\quad g_j^{M_{i,l}}\left(x_k^P, x_k^A, x_k^F\right) \leqslant 0 \quad \begin{matrix} k = 1, \ldots, N_C \\ j = 1, \ldots, m^{M_i} \\ i = 0, \ldots, D \end{matrix} \tag{3b}$$

The design variables are the cable anchor positions ($x_k^P$), cross sectional areas ($x_k^A$), and prestressing forces ($x_k^F$). $L_k$ is the total length of the cable, which depends on the anchor position on the deck. The constraints $g_j^{M_i}$ refers to the $j$th design constraint of the configuration $M_i$. The total number of constraints in each configuration is expressed by $m^{M_i}$.

As each pair of cables in the crossing zone share the same anchor position on the deck, their coordinates are represented by a single design variable. Therefore, the number of design variables related to the cable anchor position corresponds to $N_P = N_C - N_{MC1}$. Consequently,

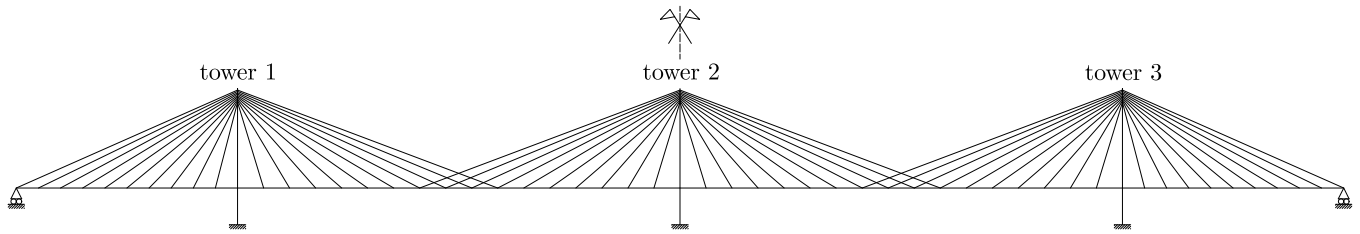


**Fig. 3.** Geometry of the generic finite element model [22].

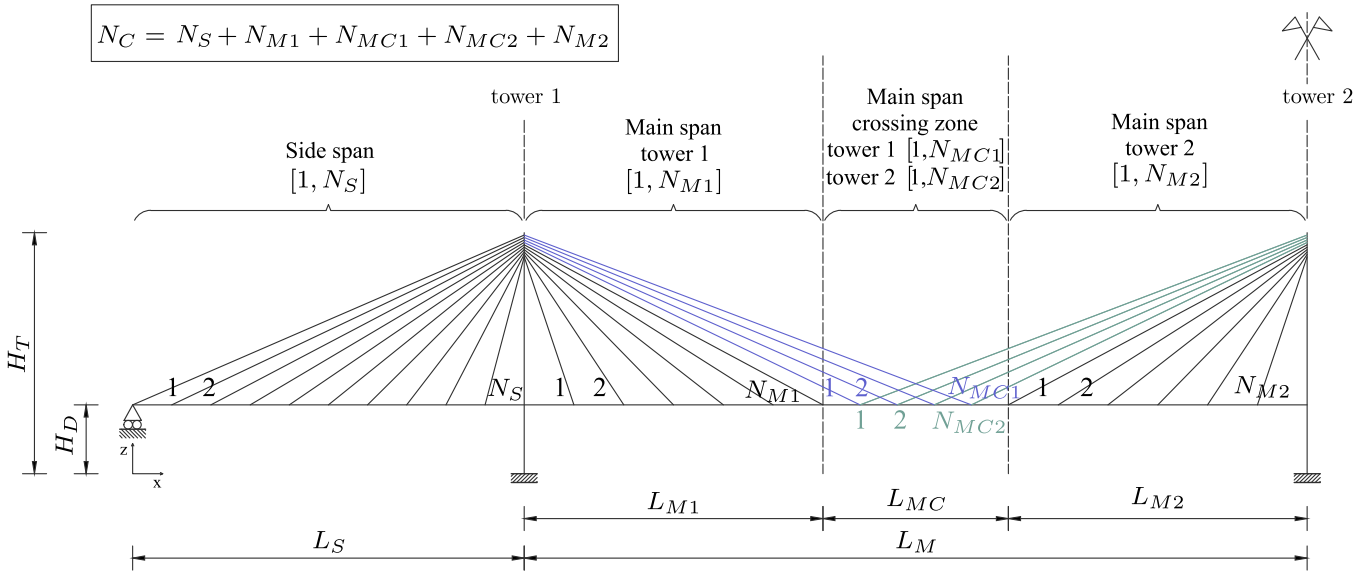


**Fig. 4.** Nomenclature used for the bridge model [22].

the total number of design variables is $N_{DV} = N_P + 2N_C$, grouped in a vector $\mathbf{x}$ as follows:

$$\mathbf{x} = [\ \underbrace{x_1, \ldots, x_{N_P}}_{\text{Cable anchor Position } (x_k^P)}\ \underbrace{, x_{N_P+1}, \ldots, x_{N_P+N_C}}_{\text{Cable Area } (x_k^A)}\ \underbrace{, x_{N_P+N_C+1}, \ldots, x_{N_P+2\cdot N_C}}_{\text{Cable prestressing Force } (x_k^F)}\ ] \quad (4)$$

As the objective is to find the optimum cable system, the number of cables in each region of the deck should be a design variable, but they have not been included in Eq. (4). The reason is that it would involve discrete variables coexisting with continuous variables, and would have to be solved with a Mixed-Integer Nonlinear Programming (MINLP) algorithm. It has been shown that for a large number of variables, these algorithms are not efficient and it is better to opt for a gradient method. An indirect way to modify the number of cables into the optimization process is to allow their area values to reach practically zero values, which has been set to $10^{-6}$ m$^2$ in this work. This approach was successfully implemented in the previous work [22]. This approach requires defining a sufficiently large initial number of cables. In this way, the areas of the unnecessary cables will converge to negligible values as the objective is to minimize their steel volume. This directly influences the cost of the cable system, since apart from minimizing the volume of material, the number of anchorages will also be reduced.

A MATLAB code was implemented to perform the optimization process. Initially, the code defines the input data of the Python script, which generates the $D + 1$ finite elements models (mechanical properties, geometry, meshing and design variables), and the optimization parameters. Then, the optimization is carried out using the Sequential Quadratic Programming (SQP) algorithm implemented in the MATLAB function *fmincon*. During the optimization process, the Python script is externally run through the Abaqus software to obtain the structural responses and evaluate the design constraints. The intact model has to be analyzed first in order to obtain the internal forces of the cables $F_{\text{cable},k}^{M_{0,I}}$; $k = 1, \ldots, N_T$. After the analysis of the intact model, the impact forces can be computed and applied to the damaged models, which are launched in parallel to evaluate their design constraints. After this process, the optimum design is reached if all design constraints are satisfied and the objective function converges. Otherwise, the design variables $\mathbf{x}$ are updated by the algorithm and a new iteration starts. The sensitivity analysis needed for this gradient-based optimization algorithm was carried out using the finite difference method, by performing a fully nonlinear analysis for each perturbation of design variables. A flowchart of the methodology used for the fail-safe optimization is shown in Fig. 6.

As mentioned earlier, a lower bound for the cross-sectional area equal to $10^{-6}$ m$^2$ was set in order to avoid the use of discrete design variables. Although mathematically the final design would be feasible, from an engineering point of view, the cross-sectional area of some cables may be so low that their manufacture would not be feasible. Therefore, a limit must be established at which the cross-sectional area is considered workable ($lb^W$). After the optimization process, a new analysis of all configurations removing the cables whose areas are lower than $lb^W$ must be done in order to recheck the design constraints.

## 4. Application example: The Queensferry Crossing bridge

The fail-safe optimization strategy described in Section 3.2 is applied to the cable-stayed part of the Queensferry Crossing bridge, also known as Forth Replacement Crossing. The bridge, with a total length of 2.64 km, is the longest three-tower cable-stayed bridge in the world and also the largest one that features crossed cables in the mid-spans. The cable-stayed part comprises three reinforced concrete towers around 200 m high and a multi-cell steel box girder deck 1950 m

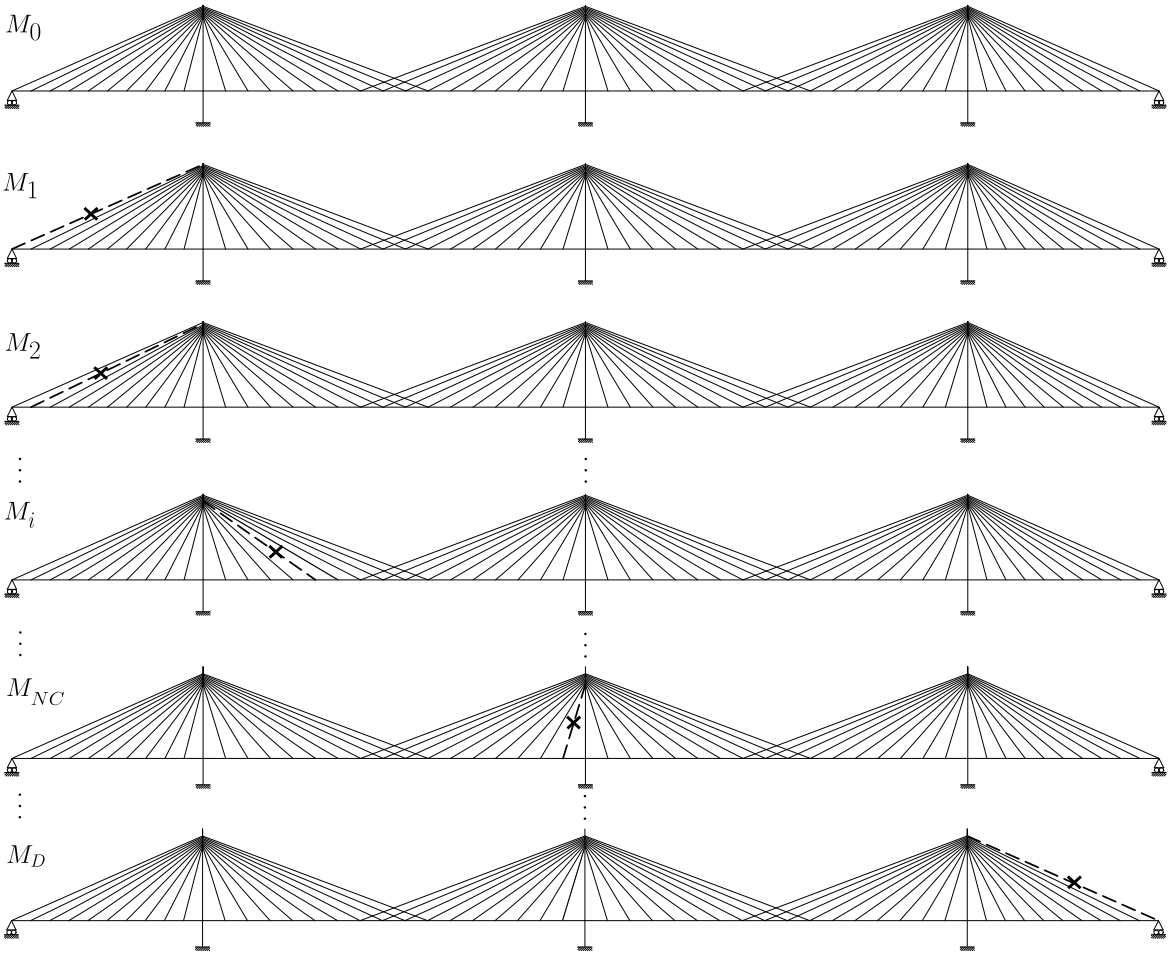


**Fig. 5.** Intact and damaged configurations in a generic cable-stayed bridge.

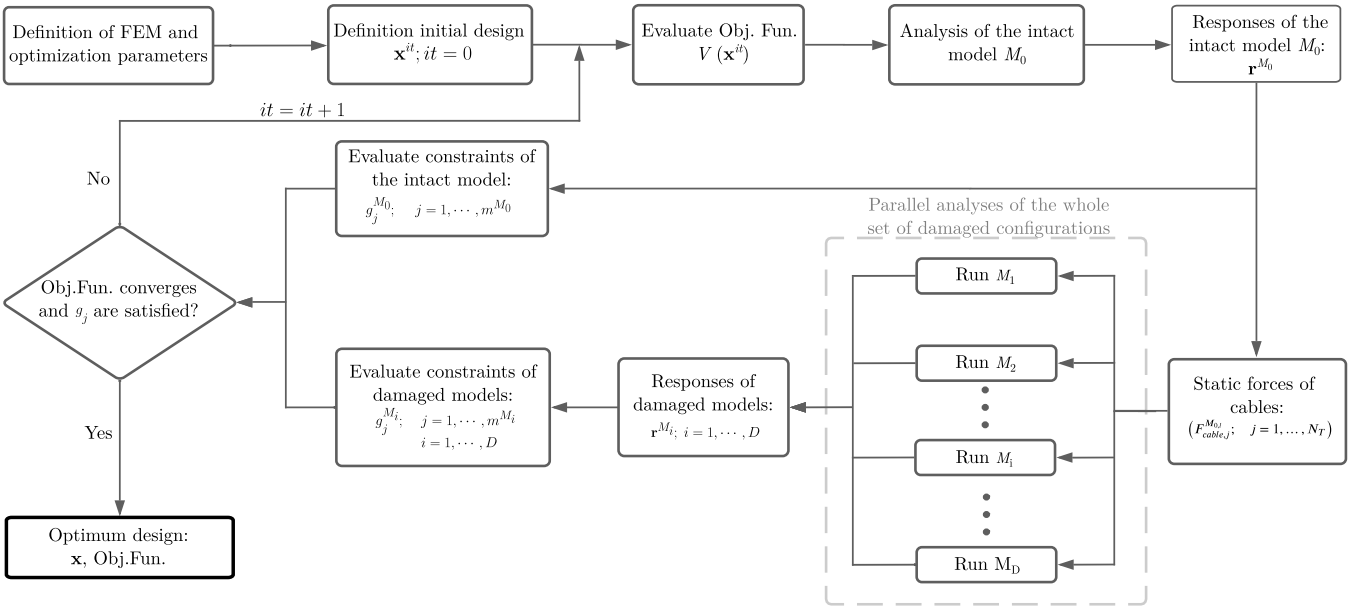


**Fig. 6.** Flowchart of the optimization problem.

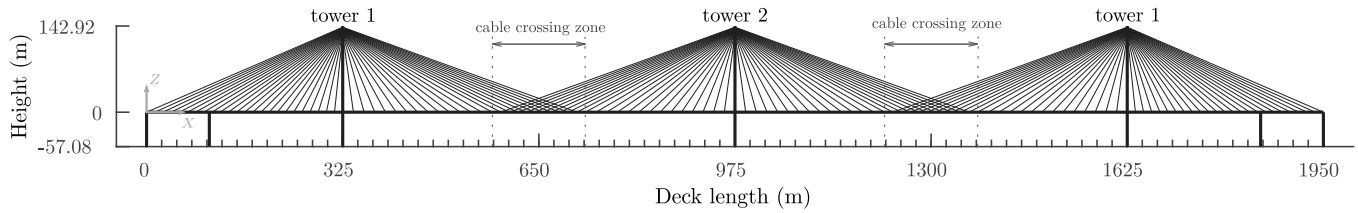


**Fig. 7.** Geometry of the generic finite element model [22].

**Table 1**
Distribution of cable pairs along the bridge.

| $N_C$ | Side span ($N_S$) | Main span ($N_M$) | | | |
|---|---|---|---|---|---|
| | | $N_{M1}$ | $N_{MC1}$ | $N_{MC2}$ | $N_{M2}$ |
| 72 | 24 | 14 | 10 | 10 | 14 |

**Table 2**
Mechanical properties of the bridge model.

| | Tower top (A–A) | Tower deck height (B–B) | Tower base (C–C) | Cables | Deck |
|---|---|---|---|---|---|
| $A$ (m$^2$) | 22.1 | 32.81 | 56.65 | Design variable | 2.00 |
| $I_z$ (m$^4$) | 118.83 | 411.61 | 1658.71 | – | 200.00 |
| $I_y$ (m$^4$) | 57.91 | 193.21 | 1386.67 | – | 7.60 |

long, being the latter composed of a back span of 221 m and one approach viaduct of 104 m. Twenty-four pairs of cables extend from each side of the tower heads to their anchorage on the deck. The cable pairs are spaced about five meters apart in the transverse direction and anchored on the deck with a longitudinal spacing of 16.2 m, resulting in 144 pairs of stays. At mid-span, the cables overlap by a length of $L_{MC} = 146$ m, which provides longitudinal stability to the central tower thus reducing the bending moments on the foundation of the tower and deck deflections under asymmetrical live loads in the main spans. According to the notation used in Section 3.1, the number of cable pairs in each deck region is listed in Table 1.

As commented before, this work uses the FEM of the Queensferry Crossing Bridge developed by Cid et al. [22]. The geometry definition of the FEM with the cable arrangement of the current bridge is shown in Fig. 7. As the FEM used is 2D, the cables of the model represent the two cable planes of the real bridge. Thus, the breakage of one cable in the model represents the breakage of a pair of cables of the real bridge. Since the cables are anchored in the center of the deck, the effect of the torsion generated by the breakage of a single cable is of minor relevance. However, in bridges with cables externally anchored to the deck, torsional effects are significant [65], and a 3D model is needed to consider them in the optimization problem.

The length of the crossing zone ($L_{MC}$) was set to 640 m, as the results presented in Ref. [22] show that longer crossing lengths reduce the weight of the cable system. The FEM was modeled in Abaqus using beam elements (B21) for the deck, towers and cables. The mesh size of deck elements was 2 m, while cables were discretized into 12 elements with a low value of bending stiffness and a density value of 7.85 t/m$^3$ to simulate the cable behavior. Cross-section of the deck and towers are shown in Figs. 8 and 9, respectively. The box girder deck section is 41.6 m wide and 4.8 m deep. The dimensions of the tower vary linearly between the sections at the base (C–C), at the deck level (B–B) and at the top of the tower (A–A). As a result, the towers were defined through beam elements of 2 m length with variable section. For that purpose, the Python script that generates the FEM computes the cross-section properties each 2 m and the corresponding variable cross-section is assigned to each beam element. The main mechanical and material properties are summarized in Table 2. The material used for deck and cables is steel with $E = 200$ GPa and $\nu = 0.3$, while for the towers has been concrete with $E = 35$ GPa and $\nu = 0.2$.

The loads considered are the dead load ($DL$), live load ($LL$), cable prestressing forces ($PS$) and cable loss dynamic forces ($CLDF$), the latter only applied in the damaged configurations. The $DL$ and $LL$ were defined as uniform loads applied on the deck with the values of 200 kN/m and 102.5 kN/m, respectively. However, in order to apply the load combination stated by the PTI in Eq. (2), the $DL$ was defined as a combination of the dead load of structural components

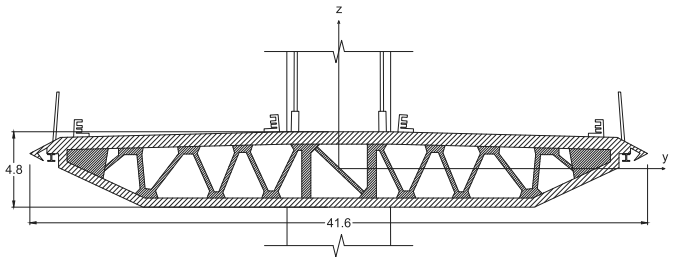


**Fig. 8.** Cross section of the deck. Units in meters [22].

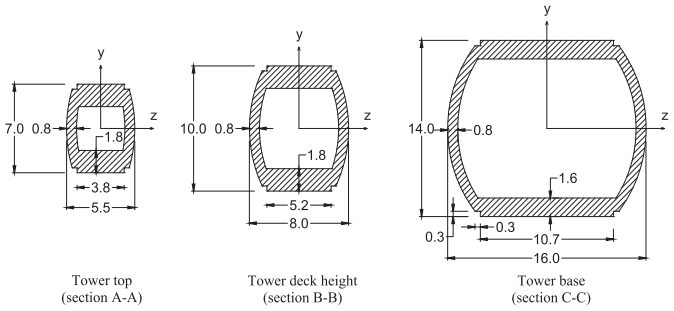


**Fig. 9.** Cross section of the towers. The local $y$-axis corresponds to the global longitudinal axis of the bridge. Units in meters [22].

($DC$) and the dead load of non-structural components ($DW$). So, the $DC$ and $DW$ were defined as the 73% and 27% of the $DL$, respectively, following the same distribution as in Messina Bridge project [66]. The $PS$, which are the design variables $x_k^F$, are modeled as negative thermal loads ($\Delta T_{\text{cable},k}$) as indicated in Eq. (5). Finally, the $CLDF$ depends on the static forces of the cables, so their values also vary during the optimization process.

$$x_k^F = \alpha \cdot \Delta T_{\text{cable},k} \cdot E_{\text{cable}} \cdot x_k^A \quad \text{with} \quad \alpha = 1 \cdot 10^{-5} \ ^\circ\text{C}^{-1} \tag{5}$$

Five load cases combining the dead load and live loads located at different sections of the bridge were considered in the previous work [22]. Among them, the load case with live loads applied on alternate spans proved to be the most critical one. Therefore, only this combination will be used in this research.

Considering that any cable of the bridge can break, the number of damaged configurations ($D$) should be equal to the number of cables of the bridge ($N_T$). However, due to the symmetry with respect to the central tower, the number of damaged configurations can be reduced to $D = N_C$, considering the symmetrical load case and the breakage of

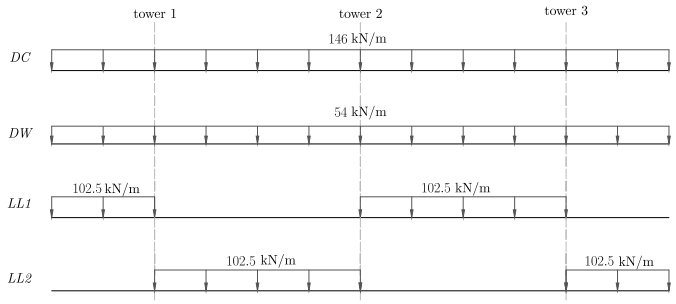


**Fig. 10.** Distribution of dead load and live load.

the symmetrical cable. This strategy reduces the number of models to be analyzed.

The set of load cases is presented in Eq. (6), according with the load combinations stated by the AASTHO [67] and PTI [27], and the distribution of dead and live loads is shown in Fig. 10. The Load Case 0 corresponds to the self-weight. The live load ($LL$) is applied in alternate spans in the Load Case 1 ($LL1$) and in the symmetrical spans in the Load Case 2 ($LL2$). Fig. 11 shows a sketch of the nomenclature used.

Intact model :

$$\text{Load Case 0 } (l=0) \quad \text{SLS}: \quad 1.00\cdot DC + 1.00\cdot DW + 1.00\cdot PS \tag{6a}$$

$$\text{ULS}: \quad 1.25\cdot DC + 1.50\cdot DW + 1.25\cdot PS \tag{6b}$$

$$\text{Load Case 1 } (l=1) \quad \text{SLS}: \quad 1.00\cdot DC + 1.00\cdot DW + 1.00\cdot LL1 + 1.00\cdot PS \tag{6c}$$

$$\text{ULS}: \quad 1.25\cdot DC + 1.50\cdot DW + 1.75\cdot LL1 + 1.25\cdot PS \tag{6d}$$

Damaged models :

$$\text{Load Case 0 } (l=0) \quad \text{EELS}: \quad 1.10\cdot DC + 1.35\cdot DW + 1.10\cdot PS + 1.10\cdot CLDF \tag{6e}$$

$$\text{Load Case 1 } (l=1) \quad \text{EELS}: \quad 1.10\cdot DC + 1.35\cdot DW + 0.75\cdot LL1 + 1.10\cdot PS + 1.10\cdot CLDF \tag{6f}$$

$$\text{Load Case 2 } (l=2) \quad \text{EELS}: \quad 1.10\cdot DC + 1.35\cdot DW + 0.75\cdot LL2 + 1.10\cdot PS + 1.10\cdot CLDF \tag{6g}$$

According to design regulations, displacements must be evaluated in the Serviceability Limit State (SLS), i.e., only in the intact model (Eqs. (6a) and (6c)). On the other hand, cables and deck stresses have to be evaluated in Ultimate Limit State (ULS) for the intact configuration (Eqs. (6b) and (6d)) and in Extreme Event Limit State (EELS) for damaged configurations (Eqs. (6e)–(6g)). Nevertheless, as the stress constraints in the deck and cables are more unfavorable when the $LL$ acts, it is enough to establish stress design constraints only in the Load Case 1 and 2. Therefore, the load combinations considered in this research are defined in Eqs. (6a), (6c), (6d), (6f) and (6g).

First, the optimization of the intact model was performed to compare the results with those obtained in the previous work [22]. This step was necessary since different regulations were considered for the application of the load cases. The steel volume of the cable system was 636.35 m$^3$, only 0.3% higher than the one obtained in the previous work (634.15 m$^3$). Fig. 12 shows the cable arrangement with the cross-sectional area values obtained, which is almost identical to the design found in the previous work. The final number of cables remaining in each span is summarized Table 3.

### 4.1. Formulation of the fail-safe optimization problem

The general methodology described in Section 3.2 to obtain the fail-safe optimum design under cable breakage is particularized for this example. The formulation of the fail-safe optimization problem is presented below:

**Table 3**
Optimum number of cables without considering cable breakage (intact model optimization).

| $N_C$ | Side span ($N_S$) | Main span ($N_M$) | | | |
|---|---|---|---|---|---|
| | | $N_{M1}$ | $N_{MC1}$ | $N_{MC2}$ | $N_{M2}$ |
| 22 | 6 | 0 | 7 | 9 | 0 |

$$\min\ V = 2\cdot\sum_{k=1}^{N_C}\left(x_k^A\cdot L_k\left(x_k^p\right)\right) \tag{7a}$$

s. t.

$$\left|w_{\text{deck},j}^{M_{0,l}}\right| \leqslant w_{\max}^{M_{0,l}} \qquad j=1,\ldots,N_D \qquad l=0,1 \tag{7b}$$

$$\left|u_{\text{tower},\ p}^{M_{0,l}}\right| \leqslant u_{\max}^{M_{0,l}} \qquad p=1,2,3 \qquad l=0,1 \tag{7c}$$

$$0 < \sigma_{\text{cable},k}^{M_{i,l}} \leqslant \sigma_{\text{cable, max}} \qquad k=1,\ldots,N_T\ /\ k\neq i \qquad i=0,\ldots,D \qquad l=1,2 \tag{7d}$$

$$\sigma_{\text{C, deck}} \leqslant \sigma_{\text{top,deck},\ j}^{M_{i,l}} \leqslant \sigma_{\text{T, deck}} \qquad j=1,\ldots,E_D \qquad i=0,\ldots,D \qquad l=1,2 \tag{7e}$$

$$\sigma_{\text{C, deck}} \leqslant \sigma_{\text{bottom,deck},\ j}^{M_{i,l}} \leqslant \sigma_{\text{T, deck}} \qquad j=1,\ldots,E_D \qquad i=0,\ldots,D \qquad l=1,2 \tag{7f}$$

$$\left|x_{k+1}-x_k\right| \geqslant d_{\min} \qquad k=1,\ldots,N_P-1 \tag{7g}$$

Eq. (7a) refers to the objective function to be minimized, which is the volume of the cable system. From Eq. (7b) to Eq. (7f), the superscripts $M_i$ and $l$ refer to the configuration and the load case, respectively, being $M_0$ the intact model and $M_1,\ldots,M_D$ the damaged models. In Eq. (7b), $w_{\text{deck},j}^{M_{0,l}}$ is the deflection of the node $j$ in the deck for the load case $l$, $w_{\max}^{M_{0,l}}$ is the maximum allowable deflection in the deck, which depends on the load case considered, and $N_D$ is the total number of deck nodes in which the displacements are checked. In Eq. (7c) $u_{\text{tower},\ p}^{M_{0,l}}$ is the horizontal displacement at the tower head $p$ and $u_{\max}^{M_{0,l}}$ is the allowed limit value. As can be seen, displacement constraints are only evaluated for the intact model in the Load Case 1 and not in the Load Case 2, due to the symmetry of the structure. In Eq. (7d), $\sigma_{\text{cable},k}^{M_{i,l}}$ is the tensile stress in cable $k$, $\sigma_{\text{cable max}}$ is the maximum allowable tensile stress in cables and $N_T$ is the total number of cables. It should be noted that the stress of the broken cable ($k=i$) is not taken into account. In Eqs. (7e) and (7f), $\sigma_{\text{bottom,deck},j}^{M_{i,l}}$ and $\sigma_{\text{top,deck},\ j}^{M_{i,l}}$ are the normal stresses in the top and bottom fiber of the deck in $j$th element and $E_D$ is the number of elements of the deck in which stresses are checked. $\sigma_{\text{C, deck}}$ and $\sigma_{\text{T, deck}}$ are the limits for compression and tension in the deck. Finally, in Eq. (7g) $d_{\min}$ represents the minimum distance between the anchor position of two consecutive cables.

Regarding to the side constraints of the design variables, the cable anchor positions must be within the corresponding deck region, as shown in Fig. 4. The lower bound of cable areas is $10^{-6}$ m$^2$ and the upper bound is 0.1 m$^2$. A workable area limit, $lb^w = 0.0025$ m$^2$, was considered. The limits of each constraint type are summarized in Table 4, being $L_S = 325$ m, $L_M = 650$ m and $H_T = 200$ m. An ultimate tensile strength for the cables of $f_u = 1860$ MPa was adopted, as stated by the PTI [27]. Regarding to stresses in the deck, a more restrictive compression limit (200 MPa) than the tensile limit (300 MPa) was imposed to prevent buckling in a simplified manner. The minimum distance between two consecutive cables was set to 5 m.

Deck vertical displacements are evaluated every four nodes of the FEM, which corresponds to each eight meters ($N_D = 243$). Deck stresses are also computed every four elements ($E_D = 242$). However, to reduce the number of constraints, the deck has been divided into 16 regions along its length and the maximum and minimum stresses for each region are used to evaluate the design constraints. Fig. 13 shows a scheme of the regions considered.

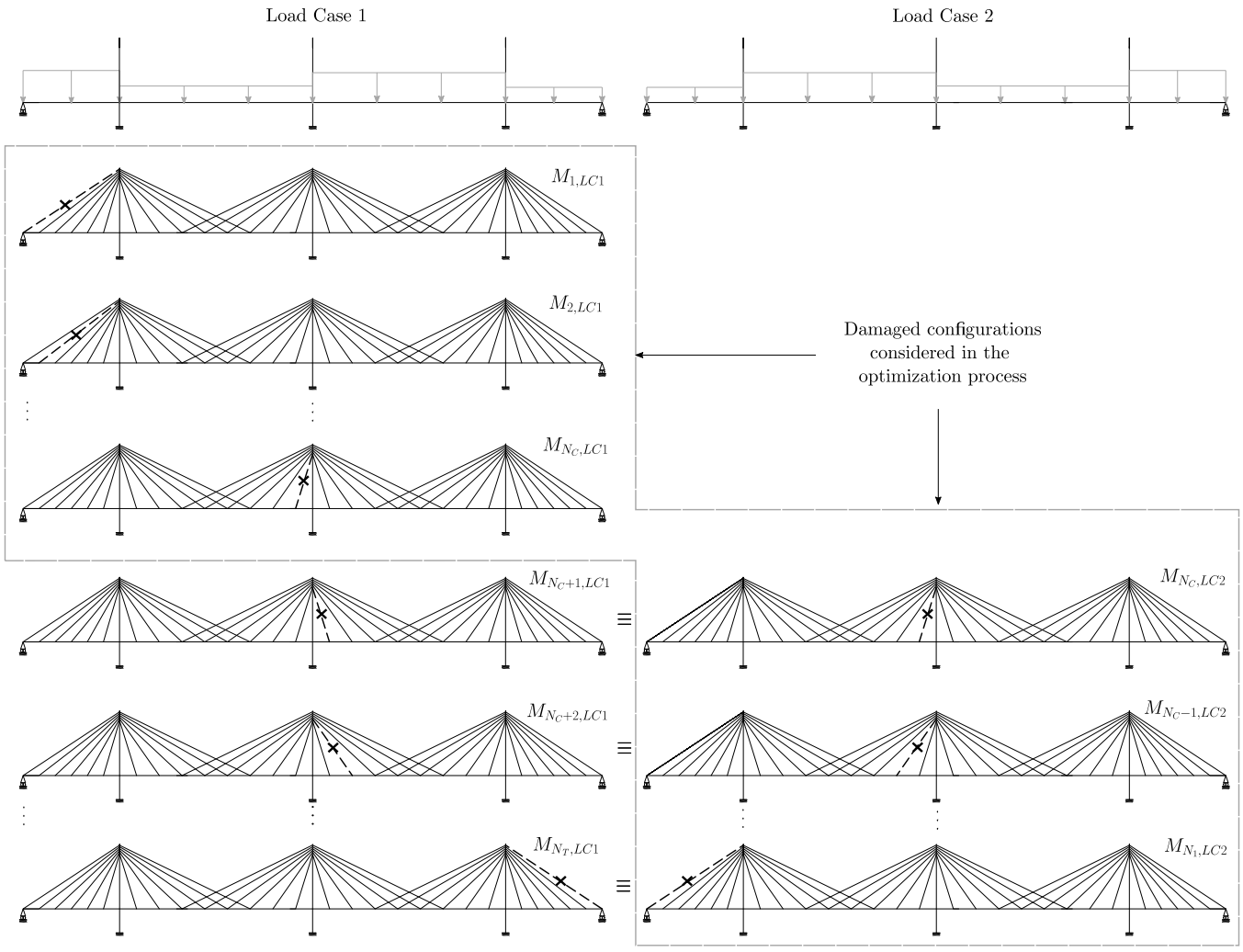


**Fig. 11.** Strategy to reduce the number of damaged models to be analyzed ($N_C$ models and two $LC$ instead of $N_T$ models and one $LC$).

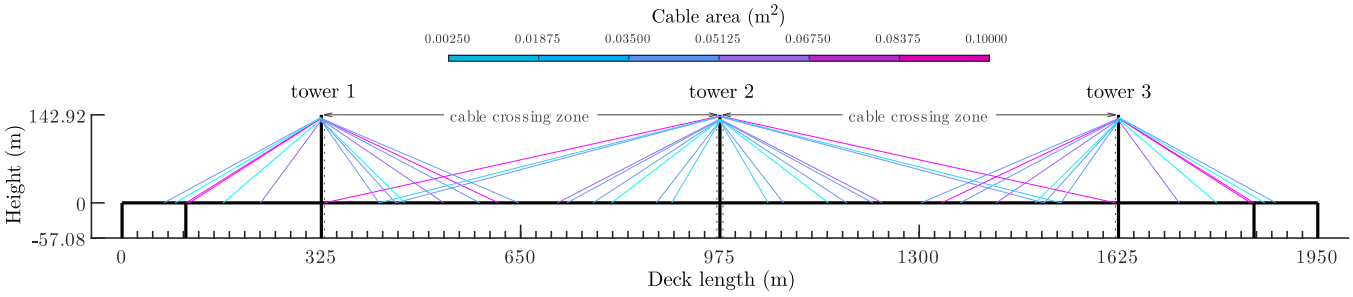


**Fig. 12.** Optimum cable layout and cross-sectional areas without considering cable breakage (intact model optimization).

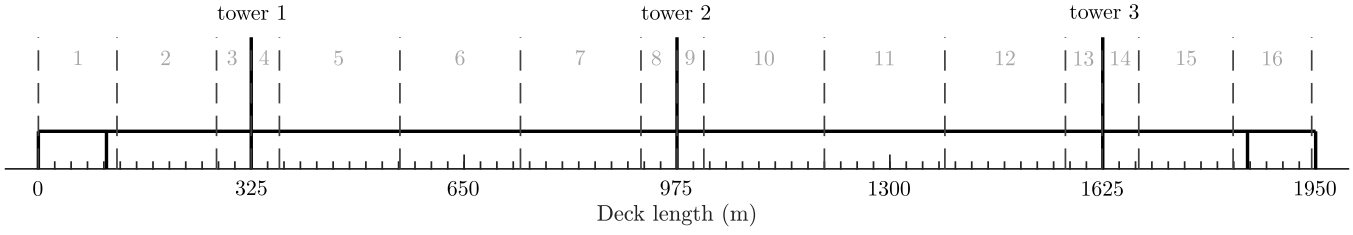


**Fig. 13.** Regions considered to evaluate stress constraints of stress on the deck.

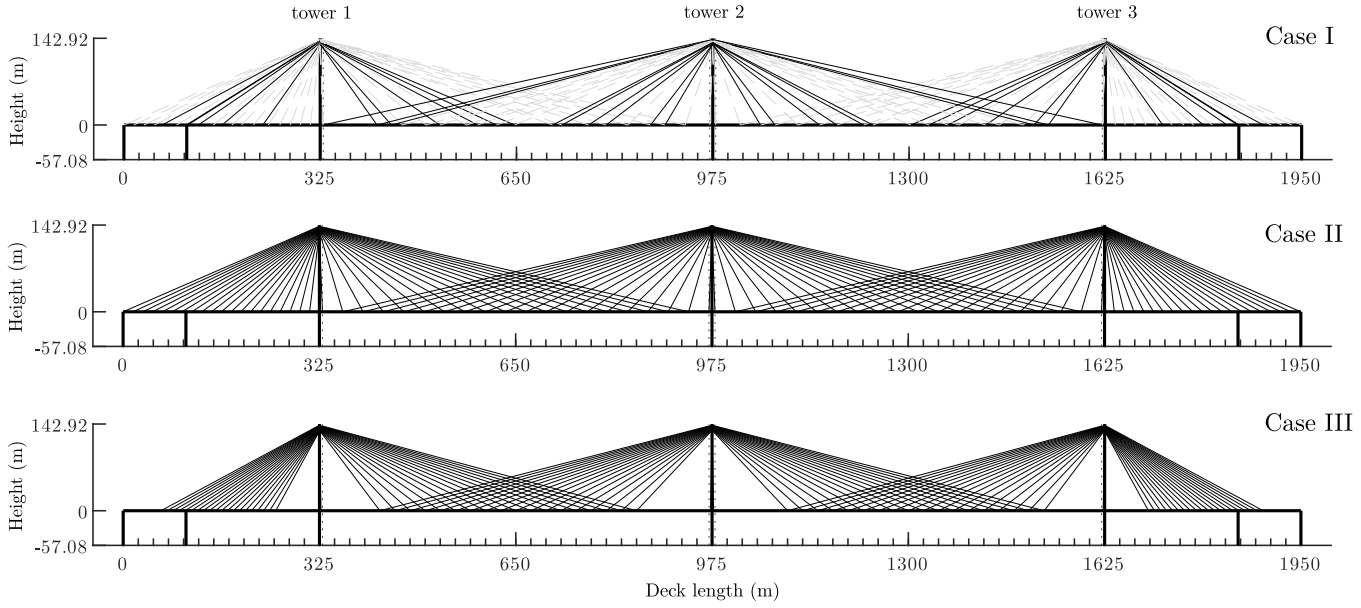


**Fig. 14.** Cable arrangement of the three initial design cases.

**Table 4**
Limit values for the structural responses.

| (a) Displacements on deck and towers | | | | | |
|---|---|---|---|---|---|
| Side span | | Main span | | | |
| $w_{\max}^{M_{0,0}}$ (m) | $w_{\max}^{M_{0,1}}$ (m) | $w_{\max}^{M_{0,0}}$ (m) | $w_{\max}^{M_{0,1}}$ (m) | $u_{\max}^{M_{0,0}}$ (m) | $u_{\max}^{M_{0,1}}$ (m) |
| $L_S/7500$ | $L_S/500$ | $L_M/7500$ | $L_S/500$ | $H_T/7500$ | $H_T/500$ |

| (b) Stresses in cables and deck, and minimum gap between cables | | | |
|---|---|---|---|
| $\sigma_{\text{cable,max}}$ (MPa) | $\sigma_{\text{T,deck}}$ (MPa) | $\sigma_{\text{C,deck}}$ (MPa) | $d_{\min}$ (m) |
| $0.45{\cdot}f_u$ | 300 | −200 | 5 |

**Table 5**
Number of cables in the three initial design cases.

| $N_C$ | Side span ($N_S$) | Main span ($N_M$) | | | |
|---|---|---|---|---|---|
| | | $N_{M1}$ | $N_{MC1}$ | $N_{MC2}$ | $N_{M2}$ |
| 58 | 20 | 1 | 18 | 18 | 1 |

Before proceeding to the optimization process, three initial designs were defined using different cable anchor positions, areas and prestressing forces. In all of them, an initial number of cables $N_C = 58$ were set, distributed as indicated in Table 5. The first initial design (Case I) corresponds to the result of the optimization of the intact model done by Cid et al. [22]. In the second initial design (Case II) cables are equally spaced along each span. Finally, Case III is similar to Case II, but cables are more concentrated in the center of each span. The layout of each case is shown in Fig. 14, where cables represented by dashed lines have areas below the $lb^w$.

### 4.2. Numerical results of the fail-safe optimization

This section presents the optimization results for the three initial designs described above. Fig. 15 shows the final cable arrangements as well as the cable area distribution, and Fig. 16 shows the evolution of the objective function. At first glance, it can be seen that the optimum cable layout solution is similar for the three optimization cases.

The final steel volume of the cable system is summarized in Table 6, where the number in brackets represents the volume increment with respect to the solution without considering cable breakage (636.25 m$^3$). Cases I and II result in 719.76 m$^3$ and 720.03 m$^3$, respectively. This implies a penalty in the steel volume of approximately 13% when considering the cable breakage in the optimization process. On the other hand, Case III leads to a slightly heavier result than in the two previous cases, increasing the penalty up to 20%.

**Table 6**
Optimum volume of the fail-safe design.

| | Case I | Case II | Case III |
|---|---|---|---|
| Fail-safe optimization | 719.76 (+13.11%) | 720.03 (+13.15%) | 771.97 (+21.31%) |

**Table 7**
Final number of cables at the fail-safe optimum design in the half length of the Queensferry Crossing.

| Case | $N_C$ | Side span ($N_S$) | Main span ($N_M$) | | | |
|---|---|---|---|---|---|---|
| | | | $N_{M1}$ | $N_{MC1}$ | $N_{MC2}$ | $N_{M2}$ |
| I | 36 (+14) | 14 (+8) | 0 | 9 (+2) | 12 (+3) | 1 (+1) |
| II | 36 (+14) | 14 (+8) | 0 | 9 (+2) | 12 (+3) | 1 (+1) |
| III | 37 (+15) | 14 (+8) | 0 | 12 (+5) | 10 (+1) | 1 (+1) |

Table 7 summarizes the number of cables obtained for the three optimization cases and each deck region. The number in brackets indicates the increase with respect to the optimum design without taking into account a cable breakage scenario. Cases I and II converge to $N_C = 36$, while Case III leads to $N_C = 37$. This means an increase of 14, 14 and 15 cables, respectively. From these results it can be drawn that, despite of minimizing only the volume of steel, a reduction in the total cost of the cable system has been indirectly achieved. This happens because during the optimization process, it is more advantageous to slightly increase the area of the existing cables than to add new ones, which translates into savings associated with the number of cables, and therefore savings in installation costs.

The number of active constraints are summarized in Table 8. From the 21,779 design constraints, 227, 226, and 239 correspond to active constraints in Cases I, II, and III, respectively. In addition, it can be seen how most of them are cable stresses in the damaged models.

Since Case I provides the fail-safe design with the lowest volume, the results for this case will be analyzed in more detail below. However,

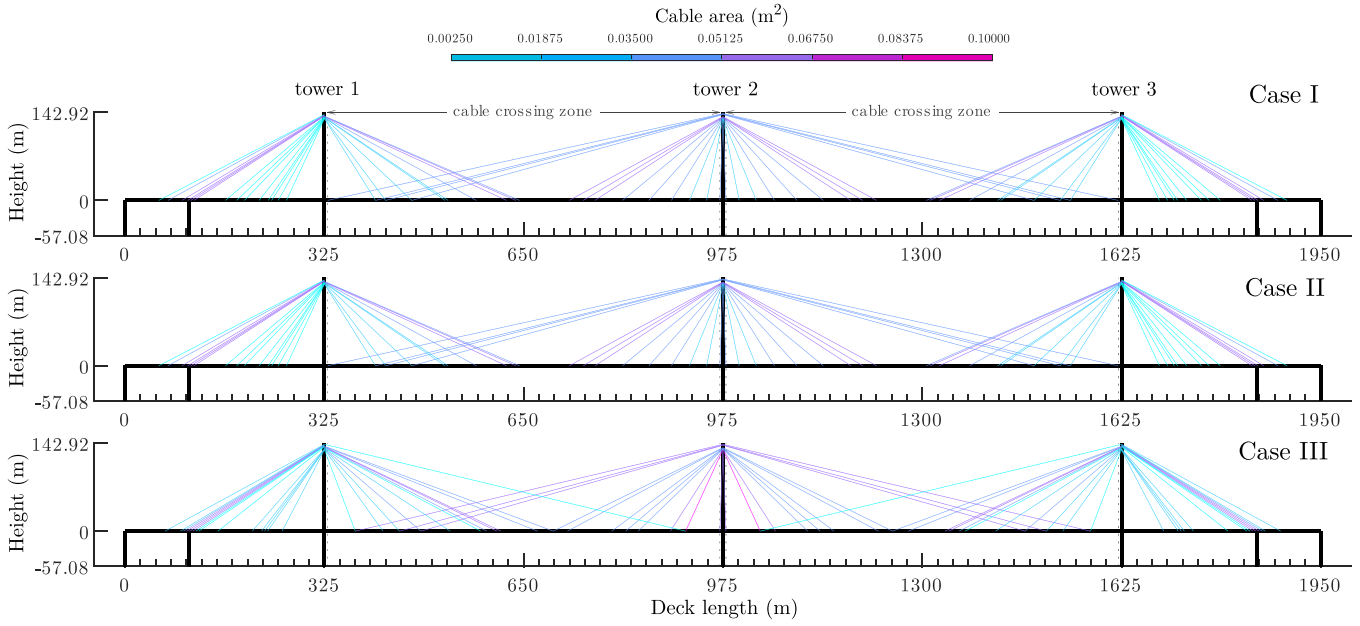


**Fig. 15.** Optimum cable area distribution for the fail-safe optimization.

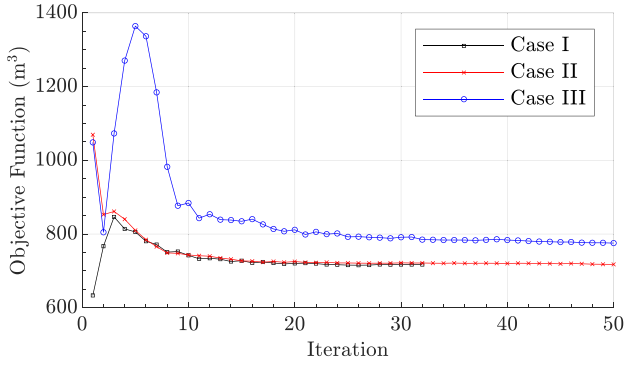


**Fig. 16.** Evolution of the objective function for the fail-safe optimization.

**Table 8**
Number of active constraints.

| | Total number of constraints | Active constraints | | | | | |
|---|---|---|---|---|---|---|---|
| | | Case I | | Case II | | Case III | |
| | | $M_0$ | $M_i$ | $M_0$ | $M_i$ | $M_0$ | $M_i$ |
| $w_{\text{deck}}$ | 486 | 67 | – | 65 | – | 76 | – |
| $u_{\text{tower}}$ | 6 | 1 | – | 1 | – | 1 | – |
| $\sigma_{\text{cable}}$ | 13456 | 8 | 123 | 8 | 123 | 13 | 111 |
| $\sigma_{\text{deck}}$ | 7488 | 1 | 24 | 1 | 25 | 2 | 24 |
| Cable spacing | 343 | 3 | – | 3 | – | 12 | – |
| Total | 21779 | 80 | 147 | 78 | 148 | 104 | 135 |

the conclusions drawn are broadly similar for the other two cases. First, the cable arrangement of the intact model and fail-safe optimization are shown together in Fig. 17. Analyzing both cable arrangements, it can be observed that they follow a similar pattern, reminiscent the Ting Kau bridge. The main feature of both cable layouts is the existence of a group of cables of great length anchored to the central tower and the deck near the side towers. In multi-span cable-stayed bridges, the control the horizontal displacement in central tower head is crucial for an adequate behavior of the structure.

The main difference between both designs lies in how the cable areas are distributed. Without the requirement for cable breakage, the design ensures compliance with the constraints by using fewer cables, some of which reach the upper area limit (0.1 $m^2$). However, in the fail-safe design, the areas of these cables are distributed over more cables with smaller areas to meet the design constraints associated with damaged configurations. Fig. 18 presents three graphs showing the cable anchorage positions, areas, and prestressing forces for the initial and fail-safe optimum designs. It should be noted that these values are represented only for the left half of the bridge, taking advantage of its symmetry with respect to the central tower. The numerical values of the design variables are also summarized in Table 9. It can be observed that 22 cables have area values significantly below the workable area limit, $lb^w = 0.0025$ $m^2$, hence they are considering as non-existing cables. Indeed, it is important to remark that 15 cables reached their minimum area value of $10^{-6}$ $m^2$. After the removal of these 22 cables from the FEM, it was found that their contribution was negligible as the active constraints remain unchanged. Thus, from a size optimization approach, a structure with a different topology has been achieved, since the number of cables has been reduced from 58 to 36 and their anchorage position on the deck have also changed.

Analyzing Figs. 17 and 18, the areas of the cables in the lateral spans can be divided into two distinct groups: cables located at $x^P$=[50 m, 120 m] and cables located between $x^P$=150 m and the first tower location. In the first group, the cables have area values ranging from 0.04 $m^2$ and 0.06 $m^2$. Most of them are located around the intermediate pier of the lateral span, which acts as a fixed anchorage point to control the horizontal displacement of the tower head in the lateral towers. In the second group, cable areas are reduced to values of around 0.015 $m^2$, being their main task to provide vertical support to the deck.

In the main spans, there is a group of 4 cables of great length and similar areas around 0.04 $m^2$. As explained before the main purpose is to brace the central tower head. Analyzing the layout of the remaining cables in the main spans, a fan-shaped distribution can be observed, reminding the standard configuration of a cable-stayed bridge. The areas of these cables grow from the towers towards the center of the span, with areas between 0.02 $m^2$ and 0.055 $m^2$. Regarding the prestressing forces, it can be seen that the cables with bigger area have a higher prestressing force, with values between 15000 kN and 20000 kN. The cables of smaller area in the lateral spans reach prestressing forces between 4000 kN and 8000 kN approximately.

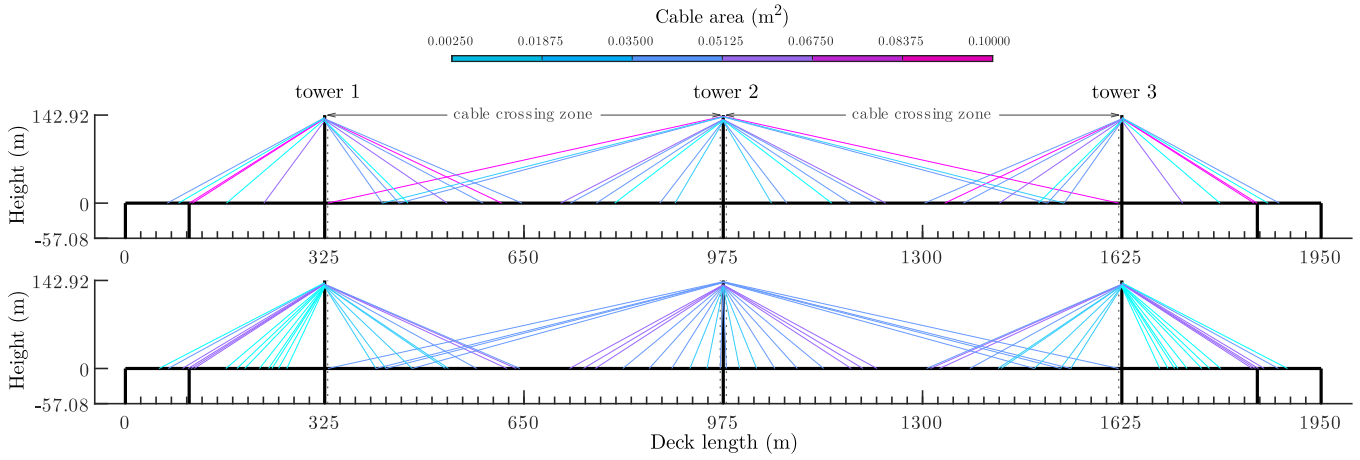


**Fig. 17.** Comparison of the optimum cable arrangement without (top) and with (bottom) fail-safe requirement under cable breakage.

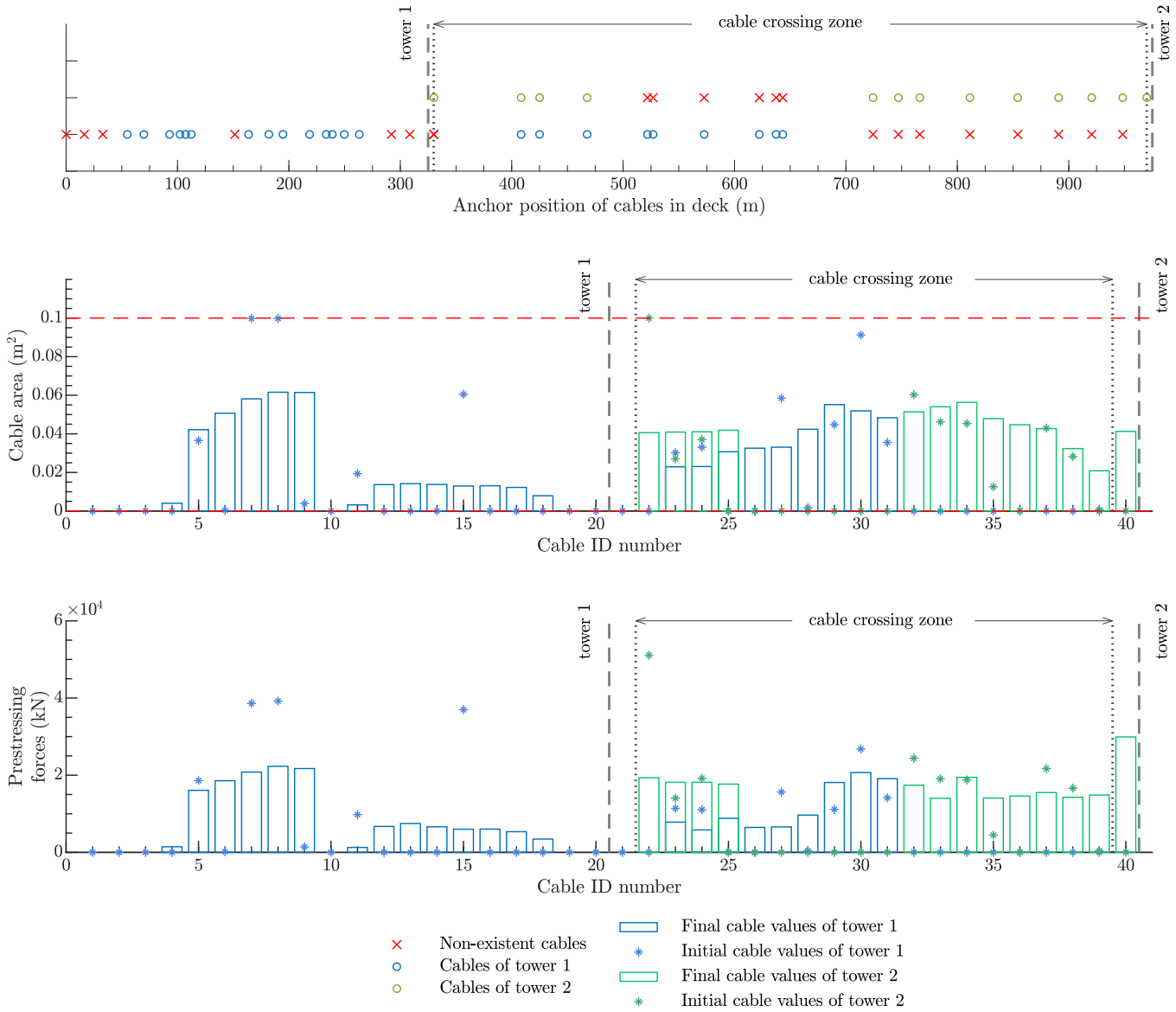


**Fig. 18.** Initial and final values of the design variables for the Case I.

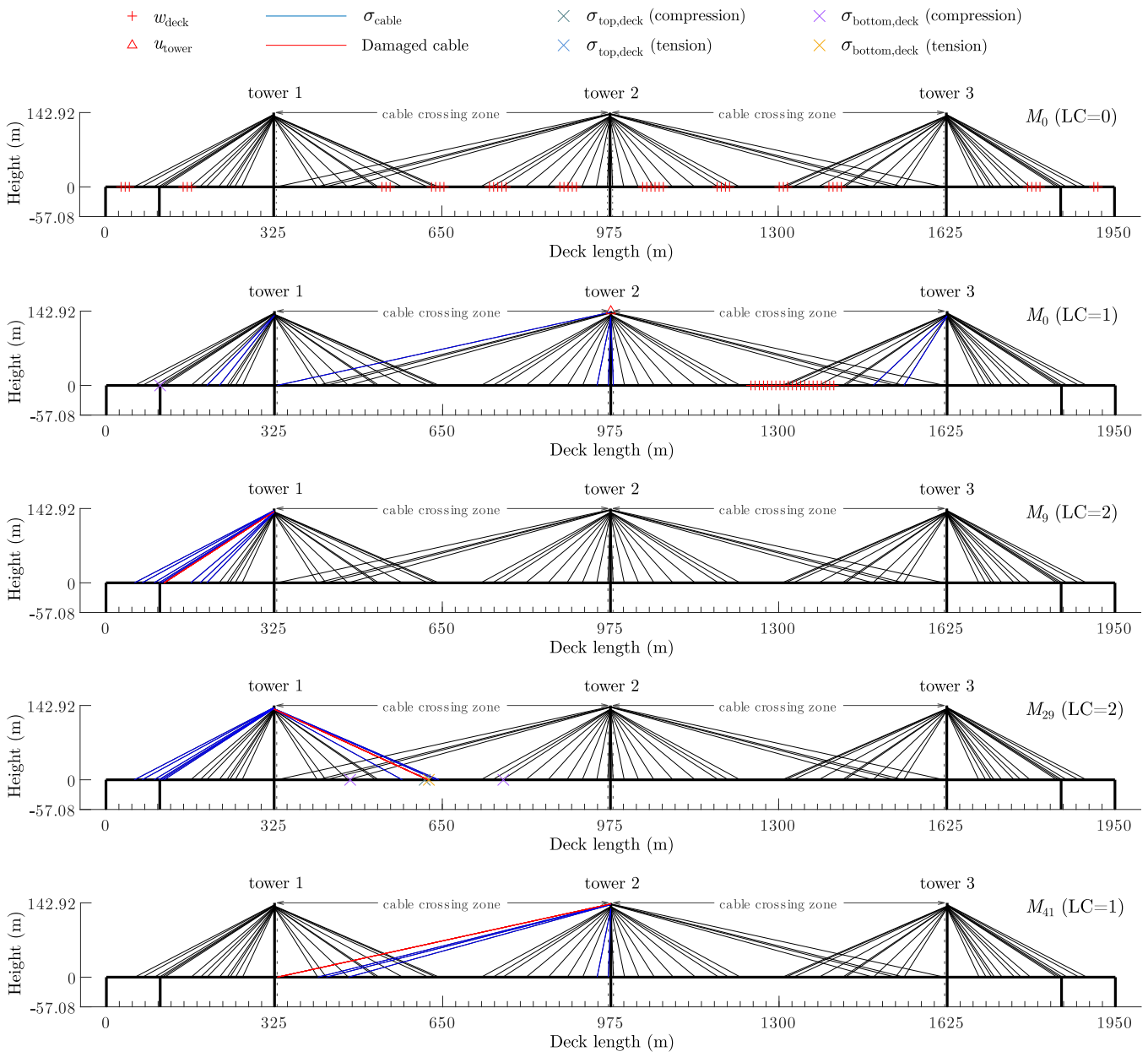


**Fig. 19.** Active constraints of the most relevant configurations for the fail-safe optimization.

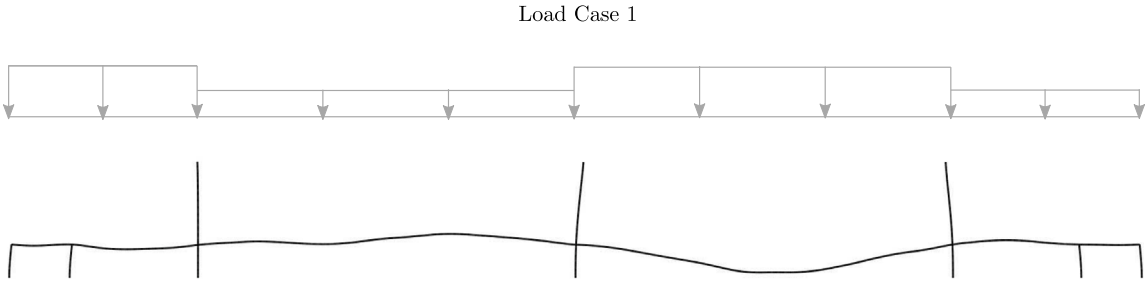


**Fig. 20.** Deformed shaped in $M_0$ for the Load Case 1. Scale factor = 40.

Fig. 19 shows the active constraints for the most relevant configurations. In the intact configuration, for LC0, there are active constraints of vertical displacements in the deck in both main and lateral spans. Some cable stress constraints are also active when LC1 is applied, as well as the horizontal displacement of the central tower head. As can be seen in Fig. 20, the live load produces a horizontal displacement of the central tower towards the loaded span, thus reaching the displacement limit at the tower head and at the same time, vertical displacements in the deck are also active in the loaded span. In addition, stress constraint in cables with highest horizontal component are also active. There is also a single

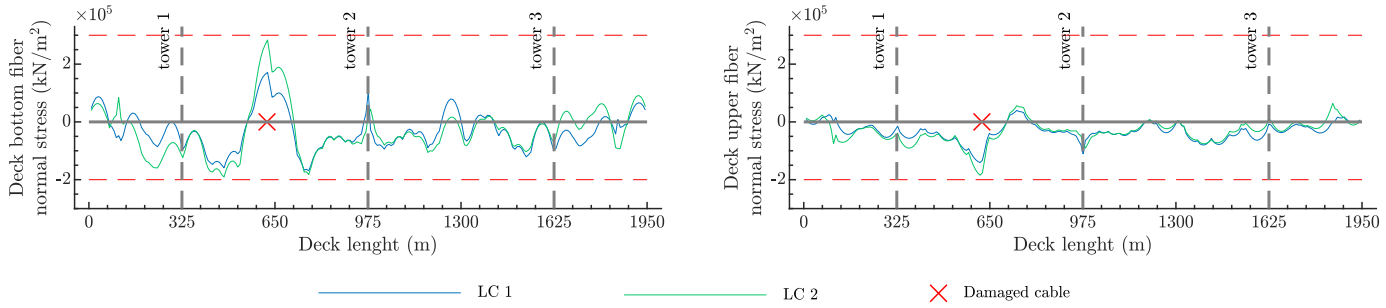


**Fig. 21.** Deck stress distribution in the damaged configuration $M_{29}$.

**Table 9**
Values of the design variables at the optimum solution.

| Side span ($N_S$) | | | | Main span tower 1 ($N_{M1}$) | | | | Main span tower 2 ($N_{M2}$) | | | |
|---|---|---|---|---|---|---|---|---|---|---|---|
| $k$ | $x_k^P$ (m) | $x_k^A$ (m$^2$) | $x_k^F$ (kN) | $k$ | $x_k^P$ (m) | $x_k^A$ (m$^2$) | $x_k^F$ (kN) | $k$ | $x_k^P$ (m) | $x_k^A$ (m$^2$) | $x_k^F$ (kN) |
| 1 | 0.11 | $10^{-6}$ | 0 | 21 | 329.90 | $10^{-6}$ | 0 | 40 | 970 | 0.0412 | 29913 |
| 2 | 16.38 | $10^{-6}$ | 0 | | | | | | | | |
| 3 | 33.02 | $10^{-6}$ | 0 | | | | | | | | |
| 4 | 54.95 | 0.0040 | 1456 | Main span ($N_{MC1}$) | | | | Main span ($N_{MC2}$) | | | |
| 5 | 69.81 | 0.0422 | 16080 | $k$ | $x_k^P$ (m) | $x_k^A$ (m$^2$) | $x_k^F$ (kN) | $k$ | $x_k^P$ (m) | $x_k^A$ (m$^2$) | $x_k^F$ (kN) |
| 6 | 92.89 | 0.0507 | 18561 | 22 | 330.25 | $10^{-6}$ | 0 | 41 | 330.25 | 0.0406 | 19347 |
| 7 | 102.26 | 0.0581 | 20800 | 23 | 408.47 | 0.0229 | 7828 | 42 | 408.47 | 0.0409 | 18155 |
| 8 | 107.26 | 0.0616 | 22291 | 24 | 425.00 | 0.0231 | 5802 | 43 | 425.00 | 0.0411 | 18174 |
| 9 | 112.35 | 0.0614 | 21722 | 25 | 467.70 | 0.0307 | 8828 | 44 | 467.70 | 0.0418 | 17687 |
| 10 | 151.46 | $1.9 \cdot 10^{-5}$ | 7 | 26 | 521.83 | 0.0326 | 6485 | 45 | 521.83 | $3 \cdot 10^{-4}$ | 101 |
| 11 | 163.80 | 0.0032 | 1280 | 27 | 526.89 | 0.0331 | 6599 | 46 | 526.89 | $10^{-4}$ | 52 |
| 12 | 182.00 | 0.0137 | 6727 | 28 | 572.74 | 0.0424 | 9648 | 47 | 572.74 | $10^{-5}$ | 5 |
| 13 | 194.65 | 0.0142 | 7463 | 29 | 622.25 | 0.0551 | 18129 | 48 | 622.25 | $10^{-6}$ | 0 |
| 14 | 218.61 | 0.0138 | 6624 | 30 | 637.30 | 0.0519 | 20696 | 49 | 637.30 | $10^{-6}$ | 0 |
| 15 | 233.48 | 0.0130 | 6008 | 31 | 643.30 | 0.0484 | 19123 | 50 | 643.30 | $5 \cdot 10^{-5}$ | 13 |
| 16 | 238.98 | 0.0131 | 6027 | 32 | 724.33 | $5 \cdot 10^{-4}$ | 218 | 51 | 724.33 | 0.0514 | 17415 |
| 17 | 249.73 | 0.0122 | 5358 | 33 | 747.09 | $10^{-4}$ | 50 | 52 | 747.09 | 0.0540 | 14002 |
| 18 | 263.19 | 0.0079 | 3445 | 34 | 766.28 | $10^{-6}$ | 0 | 53 | 766.28 | 0.0563 | 19435 |
| 19 | 292.01 | $10^{-6}$ | 0 | 35 | 811.28 | $10^{-6}$ | 0 | 54 | 811.28 | 0.0479 | 14079 |
| 20 | 308.53 | $10^{-6}$ | 0 | 36 | 854.21 | $10^{-6}$ | 0 | 55 | 854.21 | 0.0447 | 14598 |
| | | | | 37 | 890.93 | $10^{-6}$ | 0 | 56 | 890.93 | 0.0427 | 15502 |
| | | | | 38 | 920.59 | $10^{-6}$ | 0 | 57 | 920.59 | 0.0324 | 14280 |
| | | | | 39 | 948.45 | $10^{-6}$ | 0 | 58 | 948.45 | 0.0208 | 14762 |

active stress constraint in the deck around the intermediate pier of the lateral span. As for the damaged models, it can be observed that most of the active constraints occur in the vicinity of the damaged cable. In general, when a cable breaks in the lateral spans, stress constraints are activated in adjacent cables of the same span, in some cases activating up to eight cables simultaneously ($M_9$). In the main spans, the breakage of one of the four longest cables activates the stress constraints on the other three ($M_{41}$). In addition, the breakage of a cable in the center of the span anchored to tower 1 also triggers the activation of stress constraints of some cables in the side span ($M_{29}$). Regarding the deck stress constraints in damaged models, they occur when cables break in the main span. As an example, Fig. 21 shows the normal stresses in the deck for the damaged configuration $M_{29}$. As can be seen, at the location of the rupture, tensile and compression limits are reached in the bottom and upper fiber, respectively. This is due to the increase of the span length and the impact force produced by the sudden cable loss.

### 4.3. Verification of tower strength

When solving the fail-safe optimization problem, no design constraints were set on the towers. They are key elements of a cable-stayed bridge and it is necessary to verify that the new cable system design guarantees their stability. The most unfavorable scenarios correspond the breakage of the longest cables anchored at the central tower in the EELS. The reason is that the breakage of one of these cables generates a lateral impact load on the central tower head that causes a significant bending moment in the tower. Among the possible damaged models, the highest internal forces occurs on the central tower at the deck height for the model $M_{41}$, being the axial force $N_{Ed,41} = -309.73$ MN and the bending moment $M_{Ed,41} = 1676.74$ MNm. On the other hand, the corresponding internal forces in the intact model for ULS are $N_{Ed,0} = -398.40$ MN and $M_{Ed,0} = 1123.73$ MNm. As can be seen, the dynamic effect of the breakage of this cable introduces a significant increase of the internal forces in the central tower.

The verification of the tower strength has been analyzed through the axial-bending interaction diagram that has been computed using the commercial software SAP2000. This software provides the N-M diagram of a reinforced concrete section according to current regulations. A reinforcement of 690$\phi$35 was considered for this section, according to the available Refs. [68–71]. The interaction diagram was computed according to the Eurocode 2 [72]. Fig. 22 shows the reinforcement tower of the section and its interaction diagram . As can be seen, the capacity of the tower section is sufficient to resist the loads reached in the intact model (ULS) and the worst cable breakage scenario (EELS).

## 5. Conclusions

This research considers for the first time the optimization of the cable system in cable-stayed bridges considering the sudden breakage

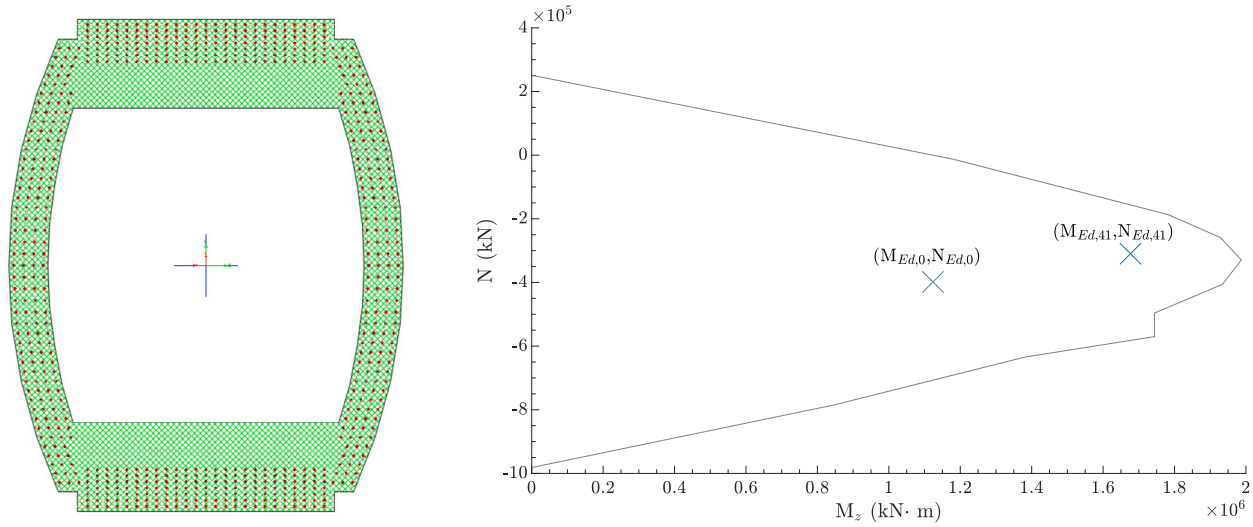


**Fig. 22.** Tower section at the deck level (left) and N-M interaction diagram (right).

of any cable. This implies taking into account the dynamic effect of this rupture in the optimization problem that aims to minimize the amount of steel used in the cables.

For this purpose, a multi-model optimization problem is proposed to handle simultaneously all possible damaged configurations with the corresponding impact loads on the deck and towers. Deck deflection, horizontal displacement at the tower heads as well as stress constraints are considered in the deck and cables. A Matlab code was developed to manage the FEM analyses performed by the Abaqus software and formulate the optimization problem.

The FEM employed in the analyses depends on the transverse layout of the cable system. When cables are externally attached to the deck, a 3D FEM should be used to take into account the torsional effects of a cable rupture. On the other hand, when cables are anchored at the center of the deck this effect is negligible and a 2D can be used instead.

The methodology has been applied to the Queensferry Crossing Bridge and the solution matches the initial expectations, as the optimum design leads to a layout with a higher number of cables and smaller area. That is, when a cable breaks, two complementary situations occur: the dynamic effect of the rupture itself and the static effect of increasing the span between two consecutive cables. Both effects are mitigated by increasing the number of cables adjacent to the one that breaks. Specifically, the optimum number of cables in the half of the bridge increases from 22 to 36 when considering the possible sudden loss of a cable with a weight increase of only 13.11%.

The solution converges to a design that has simultaneously active constraints in both the intact and damaged configurations. The highest number of constraints in the intact model corresponds to displacements in the deck and tower heads, while in damaged models there are cables with active stress constraints in the vicinity of the broken cable.

Regarding the cable layout, a group of long cables appears with the purpose of bracing the central tower head. This arrangement is observed in both designs, with and without considering cable breakage. The remaining cables follow a distribution similar to that of a traditional cable-stayed bridge, but with smaller cable spacing when compared with the optimum arrangement without considering this fail-safe requirement. This cable configuration is the result of posing a general problem where each cable anchorage position is an independent variable. Therefore, no pre-specified design pattern is forced and the cable system is allowed to vary according to the stiffness ratio between deck and tower.

## CRediT authorship contribution statement

**Noel Soto:** Software, Writing – original draft, Writing – review & editing, Visualization. **Clara Cid:** Conceptualization, Methodology, Software, Writing – original draft, Supervision, Writing – review & editing, Visualization. **Aitor Baldomir:** Conceptualization, Methodology, Writing – original draft, Supervision, Writing – review & editing. **Santiago Hernández:** Supervision.

## Declaration of competing interest

The authors declare that they have no known competing financial interests or personal relationships that could have appeared to influence the work reported in this paper.

## Data availability

No data was used for the research described in the article.

## Acknowledgments

The research leading to these results has received funding from the Galician Government through research grant ED431C 2021/33. Funding for open access charge: Universidade da Coruña/CISUG.

## References

[1] Asghar Bhatti M, Raza SM, Rajan SD. Preliminary optimal design of cable-stayed bridges. Eng Optim 1985;8(4):265–89. http://dx.doi.org/10.1080/03052158508902493.
[2] Ohkubo S, Taniwaki K. Shape and sizing optimization of cable-stayed bridges. Optim Struct Syst Ind Appl 1991;529–40.
[3] Simões LMC, Negrão JHJO. Sizing and geometry optimization of cable-stayed bridges. Comput Struct 1994;52(2):309–21. http://dx.doi.org/10.1016/0045-7949(94)90283-6.
[4] Negrão JHJO, Simões LMC. Optimization of cable-stayed bridges with three-dimensional modelling. Comput Struct 1997;64(1):741–58. http://dx.doi.org/10.1016/S0045-7949(96)00166-6.
[5] Simões LMC, Negrão JHJO. Optimization of cable-stayed bridges with box-girder decks. Adv Eng Softw 2000;31(6). http://dx.doi.org/10.1016/S0965-9978(00)00003-X.
[6] Long W, Troitsky MS, Zielinski ZA. Optimum design of cable-stayed bridges. Struct Eng Mech 1999;7(3):241–57. http://dx.doi.org/10.12989/sem.1999.7.3.241.
[7] Martins AMB, Simões LMC, Negrão JHJO. Optimum design of concrete cable-stayed bridges. Eng Optim 2016;48(5). http://dx.doi.org/10.1080/0305215X.2015.1057057.

[8] Cid Montoya M, Hernández S, Nieto F. Shape optimization of streamlined decks of cable-stayed bridges considering aeroelastic and structural constraints. J Wind Eng Ind Aerodyn 2018;177:429–55. http://dx.doi.org/10.1016/j.jweia.2017.12.018.

[9] Sun B, Zhang L, Qin Y, Xiao R. Economic performance of cable supported bridges. Struct Eng Mech 2016;59(4):621–52. http://dx.doi.org/10.12989/sem.2016.59.4.621.

[10] Qin C. Optimization of Cable-Stretching Planning in the Construction of Cable-Stayed Bridges, Vol. 19, no. 1, p. 1–20, http://dx.doi.org/10.1080/03052159208941217.

[11] Hassan MM, Nassef AO, El Damatty AA. Determination of optimum post-tensioning cable forces of cable-stayed bridges, Vol. 44, p. 248–259, http://dx.doi.org/10.1016/j.engstruct.2012.06.009.

[12] Sung Y-C, Chang D-W, Teo E-H. Optimum post-tensioning cable forces of Mau-Lo Hsi cable-stayed bridge. Eng Struct 2006;28(10):1407–17. http://dx.doi.org/10.1016/j.engstruct.2006.01.009.

[13] Lee T-Y, Kim Y-H, Kang S-W. Optimization of tensioning strategy for asymmetric cable-stayed bridge and its effect on construction process. Struct Multidiscip Optim 2008;35(6):623–9. http://dx.doi.org/10.1007/s00158-007-0172-9.

[14] Sun H, Dou Y-Z, Qian. Y-J. Optimal cable tension design for cable-stayed bridges on trust region algorithm. 2012, p. 1826–31. http://dx.doi.org/10.1061/41039(345)302.

[15] Baldomir A, Hernández S, Nieto F, Jurado JA. Cable optimization of a long span cable stayed bridge in la coruña (Spain). Adv Eng Softw 2010;41(7). http://dx.doi.org/10.1016/j.advengsoft.2010.05.001.

[16] Zhang T, Bai HF. Analysis of cable-stayed bridge for APDL-based optimization. Adv Mater Res 2011;243–249:1567–72. http://dx.doi.org/10.4028/www.scientific.net/AMR.243-249.1567.

[17] Hassan MM. Optimization of stay cables in cable-stayed bridges using finite element, genetic algorithm, and B-spline combined technique. Eng Struct 2013;49. http://dx.doi.org/10.1016/j.engstruct.2012.11.036.

[18] Sun SJ, Gao J, Huang PM. Forward-calculating optimization method for determining the rational construction state of cable-stayed bridges. Adv Mater Res 2013;671–674:980–4. http://dx.doi.org/10.4028/www.scientific.net/AMR.671-674.980.

[19] Baldomir A, Tembrás E, Hernández S. Optimization of cable weight in multi-span cable-stayed bridges. application to the forth replacement crossing. In: Proceedings of multi-span large bridges. 2015.

[20] Atmaca B, Dede T, Grzywinski M. Optimization of cables size and prestressing force for a single Pylon cable-stayed bridge with Jaya algorithm. Steel Compos Struct 2020;34(6):853–62. http://dx.doi.org/10.12989/scs.2020.34.6.853.

[21] Atmaca B. Determination of proper post-tensioning cable force of cable-stayed footbridge with TLBO algorithm. Steel Compos Struct 2021;40(6):805–16. http://dx.doi.org/10.12989/scs.2021.40.6.805.

[22] Cid C, Baldomir A, Hernández S. Optimum crossing cable system in multi-span cable-stayed bridges. Eng Struct 2018;160:342–55. http://dx.doi.org/10.1016/j.engstruct.2018.01.019.

[23] Martins AMB, Simões LMC, Negrão JHJO. Optimization of cable-stayed bridges: A literature survey. Adv Eng Softw 2020;149. http://dx.doi.org/10.1016/j.advengsoft.2020.102829.

[24] Calvi GM, Moratti M, O'Reilly GJ, Scattarreggia N, Monteiro R, Malomo D, et al. Once upon a time in Italy: The Tale of the Morandi bridge. Struct Eng Int 2019;29(2):198–217. http://dx.doi.org/10.1080/10168664.2018.1558033.

[25] Rymsza J. Causes of the collapse of the Polcevera Viaduct in Genoa, Italy. Appl Sci 2021;11(17):8098. http://dx.doi.org/10.3390/app11178098.

[26] Taiwan Transportation Safety Board. Final report released on nanfangao sea-crossing bridge collapse. 2020, URL https://www.ttsb.gov.tw/english/16051/16113/16114/28249/.

[27] Post-Tensioning Institute. Recommendations for stay cable design, testing, and installation. PTI Committee DC45.1-18; 2018, URL https://www.post-tensioning.org/publications/newsroom/m/details/f/1018.aspx.

[28] Films Media Group. A Giant on the river. 2019, URL http://films.com/title/190418.

[29] Tavares SMO, de Castro PMST. An overview of fatigue in aircraft structures. Fatigue Fract Eng Mater Struct 2017;40(10):1510–29. http://dx.doi.org/10.1111/ffe.12631.

[30] Federal Aviation Administration. Damage tolerance and fatigue evaluation of structure , AC 25.571-1D. U.S. Department of Transportation; 2011.

[31] Zoli T, Woodward R. Design of long span bridges for cable loss. In: Structures and extreme events. 2005, http://dx.doi.org/10.2749/222137805796270685.

[32] Starossek U. Progressive collapse and bridge dynamics. In: National scientific seminar on dynamics and progressive collapse in cable-stayed bridges. Hanoi University of Science and Technology; 2011, p. 1–10.

[33] Wolff M, Starossek U. Cable loss and progressive collapse in cable-stayed bridges. Bridge Struct 2009;5(1):17–28. http://dx.doi.org/10.1080/15732480902775615.

[34] Cai J-g, Xu Y-x, Zhuang L-p, Feng J, Zhang J. Comparison of various procedures for progressive collapse analysis of cable-stayed bridges. J Zhejiang Univ-Sci A 2012;5(13). http://dx.doi.org/10.1631/jzus.A1100296.

[35] Mozos CM, Aparicio AC. Parametric study on the dynamic response of cable stayed bridges to the sudden failure of a stay, Part I: bending moment acting on the deck. Eng Struct 2010;32(10):3288–300. http://dx.doi.org/10.1016/j.engstruct.2010.07.003.

[36] Mozos CM, Aparicio AC. Parametric study on the dynamic response of cable stayed bridges to the sudden failure of a stay, Part II: bending moment acting on the pylons and stress on the stays. Eng Struct 2010;32(10):3301–12. http://dx.doi.org/10.1016/j.engstruct.2010.07.002.

[37] Zhou Y, Chen S. Time-progressive dynamic assessment of abrupt cable-breakage events on cable-stayed bridges. J Bridge Eng 2014;19(2):159–71. http://dx.doi.org/10.1061/(ASCE)BE.1943-5592.0000517.

[38] Zhou Y, Chen S. Numerical investigation of cable breakage events on long-span cable-stayed bridges under stochastic traffic and wind. Eng Struct 2015;C(105):299–315. http://dx.doi.org/10.1016/j.engstruct.2015.07.009.

[39] Achtziger W, Bendsøe MP. Optimal topology design of discrete structures resisting degradation effects. Struct Optim 1999;17(1):74–8. http://dx.doi.org/10.1007/BF01197715.

[40] Mohr DP, Stein I, Matzies T, Knapek CA. Redundant robust topology optimization of Truss. Opt Eng 2014;15(4):945–72. http://dx.doi.org/10.1007/s11081-013-9241-7.

[41] Stolpe M. Fail-safe Truss topology optimization. Struct Multidisc Optim 2019;60:1605–18. http://dx.doi.org/10.1007/s00158-019-02295-7.

[42] Jansen M, Lombaert G, Schevenels M, Sigmund O. Topology optimization of fail-safe structures using a simplified local damage model. Struct Multidisc Optim 2014;49(4):657–66. http://dx.doi.org/10.1007/s00158-013-1001-y.

[43] Zhou M, Fleury R. Fail-safe topology optimization. Struct Multidisc Optim 2016;54:1225–43. http://dx.doi.org/10.1007/s00158-016-1507-1.

[44] Ambrozkiewicz O, Kriegesmann B. Adaptive strategies for fail-safe topology optimization. In: Rodrigues H, Herskovits J, Mota Soares C, Araújo A, Guedes J, Folgado J, Moleiro F, Madeira JFA, editors. Engopt 2018 proceedings of the 6th international conference on engineering optimization. Cham: Springer International Publishing; 2019, p. 200–11.

[45] Wang H, Liu J, Wen G, Xie YM. The robust fail-safe topological designs based on the von Mises stress. Finite Elem Anal Des 2020;171:103376. http://dx.doi.org/10.1016/j.finel.2019.103376.

[46] Ambrozkiewicz O, Kriegesmann B. Density-based shape optimization for fail-safe design. J Comput Des Eng 2020;7:615–29. http://dx.doi.org/10.1093/jcde/qwaa044.

[47] Smith HA, Norato JA. Topology optimization of fail-safe structures via geometry projection. In: AIAA scitech 2021 forum. VIRTUAL EVENT: American Institute of Aeronautics and Astronautics; 2021, http://dx.doi.org/10.2514/6.2021-2026.

[48] Martínez-Frutos J, Ortigosa R. Risk-averse approach for topology optimization of fail-safe structures using the level-set method. Comput Mech 2021. http://dx.doi.org/10.1007/s00466-021-02058-6.

[49] Martínez-Frutos J, Ortigosa R. Robust topology optimization of continuum structures under uncertain partial collapses. Comput Struct 2021;257:106677. http://dx.doi.org/10.1016/j.compstruc.2021.106677.

[50] Wang H, Liu J, Wen G. A study on fail-safe topological design of continuum structures with stress concentration alleviation. Struct Multidiscip Optim 2022;65(6):174. http://dx.doi.org/10.1007/s00158-022-03259-0.

[51] Sun PF, Arora JS, Haug Jr EJ. Fail-safe optimal design of structures. Eng Optim 1976;2(1):43–53. http://dx.doi.org/10.1080/03052157608960596.

[52] Arora JS, Haskell DF, Govil AK. Optimal design of large structures for damage tolerance. AIAA J 1980;18(5):563–70. http://dx.doi.org/10.2514/3.7669.

[53] Nguyen DT, Arora JS. Fail-safe optimal design of complex structures with substructures. J Mech Des 1982;104(4):861–8. http://dx.doi.org/10.1115/1.3256449.

[54] Feng YYSF, Moses F. Optimum design, redundancy and reliability of structural systems. Comput Struct 1986;24(2):239–51. http://dx.doi.org/10.1016/0045-7949(86)90283-X.

[55] Baldomir A, Hernández S, Romera L, Diaz J. Size optimization of shell structures considering several incomplete configurations. In: 53rd AIAA/ASME/ASCE/AHS/ASC structures, structural dynamics and materials conference. American Institute of Aeronautics and Astronautics; 2012, http://dx.doi.org/10.2514/6.2012-1752.

[56] Cid C, Baldomir A, Hernández S, Romera L. Multi-model reliability-based design optimization of structures considering the intact configuration and several partial collapses. Struct Multidiscip Optim 2018;57(3):977–94. http://dx.doi.org/10.1007/s00158-017-1789-y.

[57] Lüdeker JK, Kriegesmann B. Fail-safe optimization of beam structures. J Comput. Des. Eng. 2019;6(3):260–8. http://dx.doi.org/10.1016/j.jcde.2019.01.004.

[58] Cid C, Baldomir A, Hernández S. Probability-damage approach for fail-safe design optimization (PDFSO). Struct Multidiscip Optim 2020;62(6):3149–63. http://dx.doi.org/10.1007/s00158-020-02660-x.

[59] Dou S, Stolpe M. On stress-constrained fail-safe structural optimization considering partial damage. Struct Multidiscip Optim 2021;63(2):929–33. http://dx.doi.org/10.1007/s00158-020-02782-2.

[60] Dou S, Stolpe M. Fail-safe optimization of tubular frame structures under stress and eigenfrequency requirements. Comput Struct 2022;258:106684. http://dx.doi.org/10.1016/j.compstruc.2021.106684.

[61] Cid C, Baldomir A, Hernández S. Reliability index–based strategy for the probability–damage approach in fail–safe design optimization ($\beta$-PDFSO). Eng Comput 2022. http://dx.doi.org/10.1007/s00366-022-01611-y.
[62] Kirby J, Zhou S, Xie YM. Optimal fail-safe Truss structures: New solutions and uncommon characteristics. Acta Mech Sinica 2022;38(6):421564. http://dx.doi.org/10.1007/s10409-022-09028-3.
[63] Wolff M, Starossek U. Robustness assessment of a cable-stayed bridge. In: IABMAS'08: international conference on bridge maintenance, safety and management. 2008, http://dx.doi.org/10.1201/9781439828434.ch442.
[64] Abaqus. Abaqus 2019 documentation. 2019.
[65] Scattarreggia N, Galik W, Calvi PM, Moratti M, Orgnoni A, Pinho R. Analytical and numerical analysis of the torsional response of the multi-cell deck of a collapsed cable-stayed bridge. Eng Struct 2022;265. http://dx.doi.org/10.1016/j.engstruct.2022.114412.
[66] Chodai Co Ltd. Ponte sullo Stretto di Messina. In: Review report on the preliminary design. 2004.
[67] Asstho. AASTHO LRFD bridge design specifications. 8th Ed. Washington State Department of Transportation; 2017, URL https://wsdot.wa.gov/publications/fulltext/Bridge/designmemos/09-2017.PDF.
[68] Romberg M, Brunton K, Castro JW, Moloney A, Robinson N, Wheeler M. Queensferry crossing, UK: towers, piers and abutments – design and construction. In: Proceedings of the institution of civil engineers - bridge engineering, Vol. 172, no. 2. 2019, http://dx.doi.org/10.1680/jbren.18.00015.
[69] Allplan Engineering. Three centuries of bridge building over the Firth of Forth. URL https://www.allplan.com/references/engineering/queensferry-crossing/.
[70] Queensferry Crossing. Forth Road and Railway Bridges – e-mosty, URL https://e-mosty.cz/queensferry-crossing-forth-road-and-railway-bridges/.
[71] Vázquez A. Tower construction in the new queensferry crossing. In: ACHE VII. 2017.
[72] Eurocode 2: Design of concrete structures | Eurocodes: Building the future, URL https://eurocodes.jrc.ec.europa.eu/EN-Eurocodes/eurocode-2-design-concrete-structures.